Palaeogeography, Palaeoclimatology, Palaeoecology 581 (2021) 110633

Contents lists available at ScienceDirect

Palaeogeography, Palaeoclimatology, Palaeoecology

journal homepage: www.elsevier.com/locate/palaeo

The Messinian of Agios Myron (Crete, Greece): A key to better understanding of diatomite formation on Gavdos (south of Crete)

Willem Jan Zachariasse [a], George Kontakiotis [b], Lucas J. Lourens [a,*], Assimina Antonarakou [b]

[a] Department of Earth Sciences, Faculty of Geoscience, Utrecht University, Vening Meinesz building A, Princetonlaan 8a, 3584 CB Utrecht, the Netherlands
[b] Department of Historical Geology and Paleontology, Faculty of Geology and Geoenvironment, National and Kapodistrian University of Athens, Panepistimiopolis, Zografou, 15784 Athens, Greece

ARTICLE INFO

Editor: A Dickson

Keywords:
Early Messinian
Sapropel-homogeneous marl cycles
Orbital tuning
Planktonic foraminifers
Stable isotopes
Paleobathymetry
Eastern Mediterranean

ABSTRACT

The Agios Myron section in the NE of the Heraklion Basin on central Crete exposes a pre-evaporitic Messinian sequence of 24 sedimentary cycles of deep-marine homogeneous and laminated marls (sapropels). Planktonic foraminiferal biostratigraphy and ash layers show that the 24 cycles in section Agios Myron correlate to cycles M79 to M102 in the well-studied and orbitally tuned Metochia section on Gavdos Island. The correlation of the cycle patterns in sections Agios Myron and Metochia not only provides tuned ages for sedimentary cycles, planktonic foraminiferal bioevents, and ash layers in Agios Myron, but also reveals that the diatomites in Metochia cycles M94-M102 have no equivalents at Agios Myron. The onset of diatomite formation on Gavdos at 6.72 Ma is shown to coincide with eutrophication and related to a restriction-imposed increase in salinity 20 kyr earlier at 6.74 Ma. Geographic differences in productivity and possibly also the better preservation potential of siliceous microfossils on the much deeper seafloor at the Metochia site are believed to explain why diatomites are present on Gavdos and absent in time-equivalent levels at Agios Myron.

1. Introduction

One of the classic reference sections for the Mediterranean Messinian is the Metochia section on Gavdos Island (located some 36 km to the S of Crete, see Fig. 1A). This section exposes a complete pre-evaporitic Messinian sequence of 56 cycles of deep marine, laminated and homogeneous marls with diatomites in the upper 21 cycles and five evaporitic limestone cycles (Krijgsman et al., 1999). Similar complete sequences have not been found so far on Crete. Some of the published sections on Crete extend to various degrees across the level which on Gavdos marks the onset of diatomite formation but lack the diatomites (Hilgen et al., 1997; Zachariasse et al., 2008; Moissette et al., 2018) though diatoms are sometimes preserved in laminated marls that are arguably or presumed to be of the same age as one of the diatomites on Gavdos (Gaudant et al., 1997; own unpublished data). In this study we report on the Messinian of the Agios Myron section, whose cyclically-bedded deep marine marls are exposed along a small road to the W of the eponymous village in the NW Heraklion Basin on central Crete (Fig. 1B,C). The reason to sample the section is that part of the cyclically-bedded unit of sapropels and homogeneous marls with three ash layers was expected to be time equivalent with the diatomite unit in the Metochia section on Gavdos. If true, then the absence of diatomites in section Agios Myron makes this section interesting to learn more about the origin of the diatomites on Gavdos. The only study done on the Gavdos diatomites so far is that of Pérez-Folgado et al. (2003) who showed that diatomite formation is related to shoaling/deepening of the nutricline during minimum/maximum precession but leave the question why diatomites suddenly begin to form unanswered. This question will be addressed in this study along with the question why 100 km further north, at Agios Myron on central Crete, no diatomites are formed.

2. Geological setting

Crete is an emerged horst of Alpine nappes and Neogene basins in the outer Hellenic arc (Fig. 1A). The Heraklion Basin on central Crete with the Agios Myron section in the NW (Fig. 1B) is the largest of these Neogene basins. The present-day extent of this basin dates from the latest Tortonian but the current high topography of the surrounding

* Corresponding author at: Department of Earth Sciences, Faculty of Geoscience, Utrecht University, Vening Meinesz building A, Princetonlaan 8a, 3584 CB Utrecht, the Netherlands.
E-mail addresses: W.J.Zachariasse@uu.nl (W.J. Zachariasse), gkontak@geol.uoa.gr (G. Kontakiotis), l.j.lourens@uu.nl (L.J. Lourens), aantonar@geol.uoa.gr (A. Antonarakou).

https://doi.org/10.1016/j.palaeo.2021.110633
Received 22 May 2021; Received in revised form 17 August 2021; Accepted 19 August 2021
Available online 28 August 2021

mountain blocks is largely shaped in the Pleistocene (Fassoulas, 2001; Roberts et al., 2013). The earliest basin on central Crete (called the Viannos Basin) is part of a large *E*-W trending and westward-draining fluvial basin that came into existence around 11 Ma (Van Hinsbergen and Meulenkamp, 2006; Zachariasse et al., 2011). This fluvial basin transformed into the deep marine Skinias Basin at ~10.5 Ma, where submergence goes together with the emplacement of chaotic mixtures of basin sediments and basement blocks (Ten Veen and Postma, 1999a; Van Hinsbergen and Meulenkamp, 2006; Zachariasse et al., 2011). The fluvial and deep marine sediments of the Viannos and Skinias Basins belong to eponymous formations described in detail by Zachariasse et al. (2011), whereas the mass wasting deposits in between were separately mapped as Illias Formation on the official geological map of Greece (IGME, 1994, 1996). Uplift and transformation of the Skinias Basin into four different fault blocks bounded by N-S and E-W normal faults is the best documented example on Crete of the transition from an early phase of basin formation dominated by N-S extension to a later one dominated by overall extension (Angelier, 1975; Ten Veen and Postma, 1999b; Fassoulas, 2001). The northern block with the Agios Myron section emerged after 9.6 Ma and remained emerged until the latest Tortonian (~7.4 Ma) except the northernmost part that became involved in the formation of the Cretan (forearc) Basin at ~8.8 Ma (Zachariasse et al., 2011).

Subsidence of the northern block to upper bathyal depths in the Early Messinian is manifested by the Agios Myron Formation. In situ gypsum is locally preserved, but most of the Lower Evaporites have been removed by subaerial erosion during (near-complete) desiccation of the Mediterranean in the latest Messinian. This so-called terminal Miocene

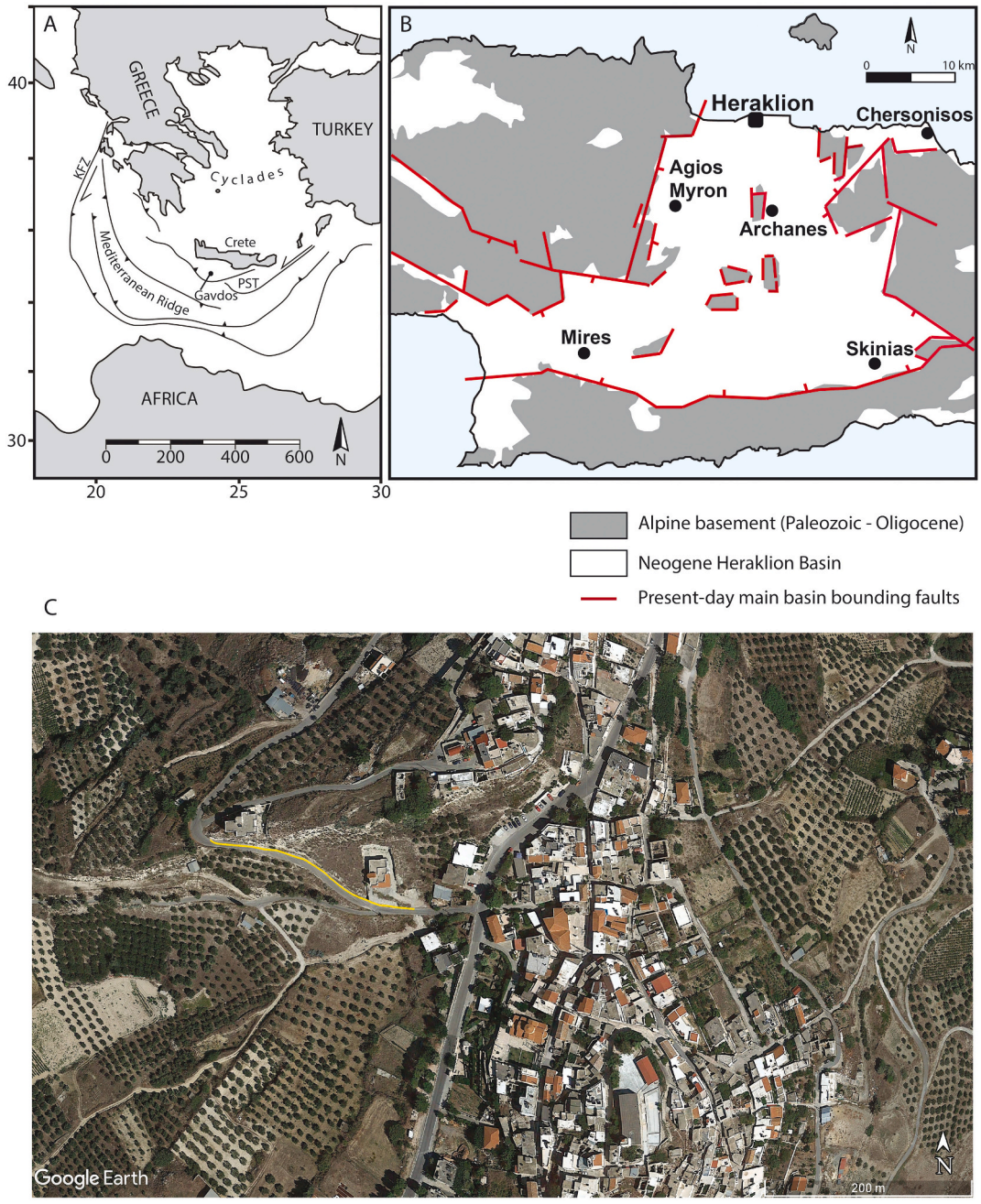

Fig. 1. (A) Map of the Aegean region with Crete and Gavdos Island (modified from Zachariasse et al., 2008). KFZ- Kefalonia Fault Zone; PST- Pliny and Strabo Trenches of the South Aegean strike-slip system; (B) Simplified geological map of central Crete (modified from Creutzburg et al., 1977); (C) Satellite image (Google Earth) showing the village of Agios Myron and the section (in yellow).

erosional unconformity is re-used as slope failure plane for submarine sliding in the Early Pliocene as is indicated by widely distributed mass wasting deposits of Lower Pliocene deep marine calcareous marls and non-marine terminal Messinian sediments (Zachariasse et al., 2008). Nevertheless, several areas in the Heraklion Basin still preserve thick series of non-marine terminal Messinian sediments; e.g., to the W of Ano Asites (Delrieu, 1990). The Heraklion Basin (and the rest of Crete) became uplifted since 5 Ma and emerged in the Late Pliocene at ~3 Ma (Van Hinsbergen and Meulenkamp, 2006; Zachariasse et al., 2008). Both the Early Pliocene mass wasting and overall uplift have been attributed to the formation of the south Aegean left-lateral strike slip system (Zachariasse et al., 2008). Along this system and the Kefalonia Fault Zone at the NW edge of the Aegean lithosphere (Fig. 1A), subducted African crust rolls back to the southwest resulting in isostatic uplift at the leading edge (Govers and Wortel, 2005).

3. The Agios Myron section

The section is located on a N-S trending fault block to the E of the Psiloritis footwall and to the W of a hanging wall block (Fig. 2). Sediments of the Agios Myron Formation in the eponymous section dip ~20° to the WNW and unconformably overly the Viannos Formation and basement flysch. The few erosional remnants of the Illias Formation overlying the Viannos Formation to the S were once covered by the Agios Myron Formation as well (Fig. 2).

The basal part of the sequence at Agios Myron is exposed below the village of Agios Myron and consists of clast-supported conglomerates of poorly sorted, rounded debris from all basement units and silts with calcrete horizons. This fluvial series is 10 m thick and passes upwards into a shallow marine series of poorly cemented sands with *Porites* coral structures (4 m) and bioturbated sandstones locally with the red coralline alga *Lithothamnion* (6 m). The non-exposed interval between the series below the village and the studied section in the W is estimated at some 12 m. The studied section is continuously exposed along an *E*-W

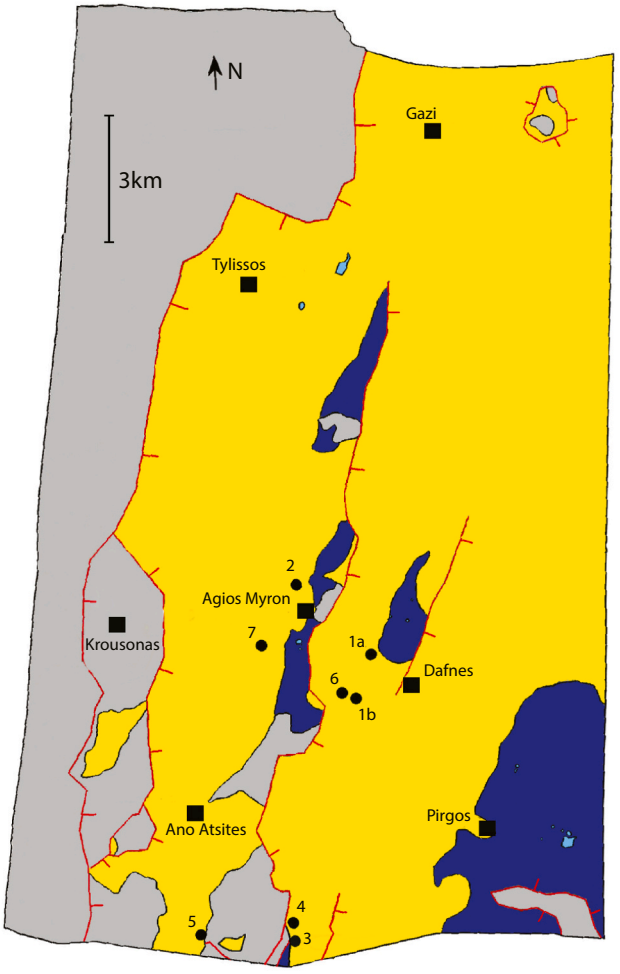

Fig. 2. Simplified geological map of the area of Agios Myron (modified from Jonkers, 1984, Delrieu, 1990 and IGME, 1994) with the Early Tortonian Viannos and Illias Fms in dark and light blue, and Messinian and younger in yellow. Normal faults in red. Black squares with names refer to villages; black dots with numbers are locations of sections discussed in 6.1 and shown in Fig. 11.

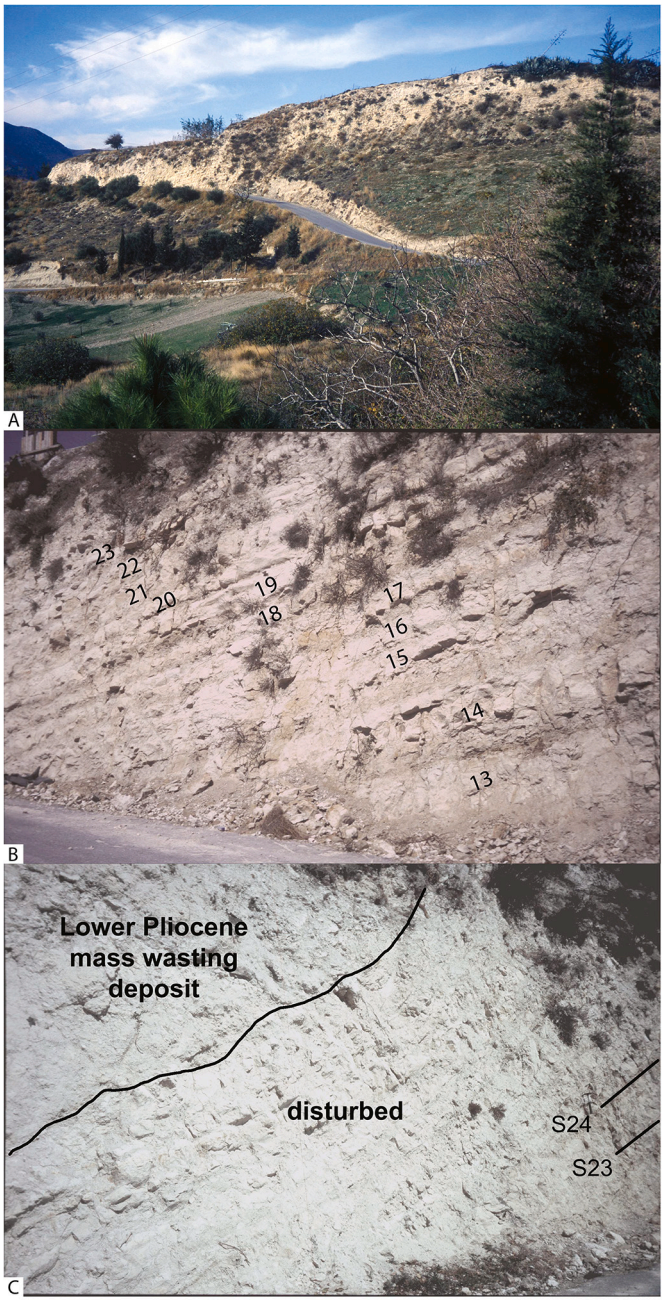

Fig. 3. (A) Agios Myron section from a distance; (B) The cyclically bedded upper part of the section. Numbers refer to AM cycles; (C) The disturbed upper 2.5 m of the cyclically bedded unit (not sampled) with Lower Pliocene mass wasting deposit on top.

road that branches off from the main road at 35° 13.977 N/25° 01.689E (see also Figs. 1C and 3A) and shown in Fig. 4A.

The first 10 m of the section consist of silty marls with some shell debris . Then follows an interval with sedimentary cycles of bluish-grey homogeneous and laminated brownish marls (sapropels) numbered AM1 to AM24 (see Fig. 3B). The homogeneous marl beds become more calcareous from cycle AM13 upwards with clearly indurated levels in the homogeneous marl beds of cycles AM19 and AM21. The upper 2.5 m of the cyclically-bedded unit is disturbed and unconformably overlain by a Lower Pliocene mass wasting deposit with azoic calciclastics and cavernous limestones from the terminal Messinian, but without Lower Pliocene sediments (see Fig. 3C). Overall, the studied section is 25 m thick and includes a few thin-bedded turbiditic sandstones and three ash layers in cycles AM6, AM8, and AM14 (Fig. 4A).

4. Materials and methods

A total of 170 samples with an average spacing of 35 cm for the silty marls without cycles and 15 cm for the cyclically bedded marls were collected in the period 2001–2003. Samples were washed over 125- and 595-μm opening sieves for foraminiferal and stable isotope studies.

Quantitative data on foraminiferal species are based on counts of 200–300 specimens in 14 randomly distributed fields of the 45-field picking tray. A principle component analysis (executed in C2 and standardized by center) was performed on the combined percentages of planktonic foraminiferal taxa in sections Agios Myron and Metochia using the software package of Juggins (2003). Semi-quantitative data on foraminiferal species are based on their numbers in 9 fields of a 45-field rectangular picking tray with F: > 20; C: 10–20; R: 3–10 and T: < 3 and > 1 specimens in 27 fields.

Stable isotopes were measured on a Thermo Gas Bench-II coupled to a Thermo Delta-V Advantage. All samples were calibrated using the in-

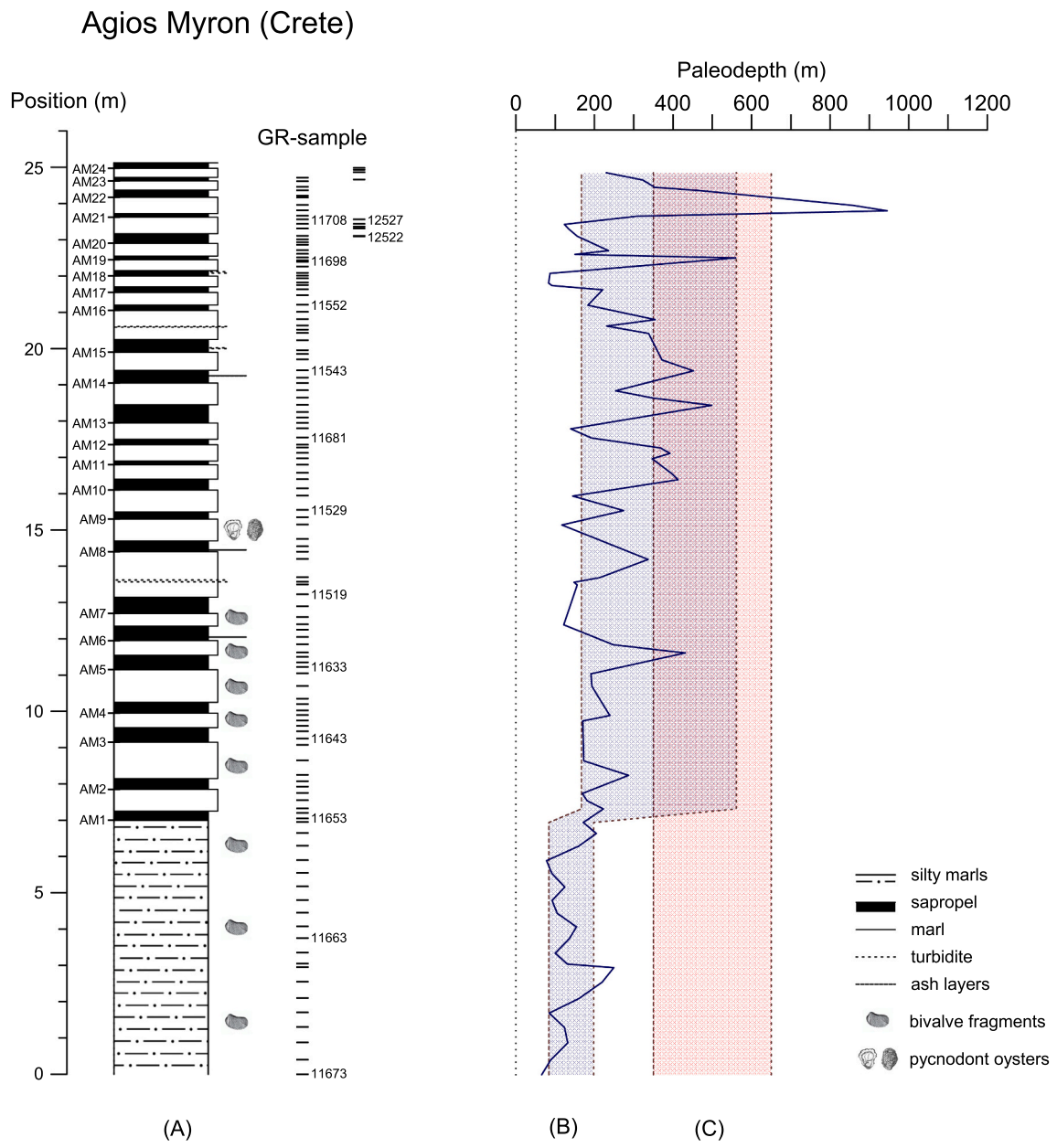

Fig. 4. (A) Agios Myron section with sedimentary cycles (numbered AM1-24), ash layers, and sample positions. The reconstruction of the depositional depth to the right of the column is based on %*P* values (B) and benthic foraminiferal depth markers (C) (see Table S1 for all data).

house standard "Naxos" and the Carrara marble "IAEA-CO-1" that is used as an international standard. Replicate analyses of samples in the past suggest that analytical precision of this set-up is 0.12‰ for carbon and 0.10‰ for oxygen isotopes. All values are reported in the standard delta notation relative to the Vienna Pee Dee Belemnite (VPDB).

The Vanadium (V) content is measured in parts per million (ppm) on 5 g subsamples which were dried, ground and digested in 5 ml HF and 5 ml HCLO4/HNO3 mixture at 90 °C. After drying, residues were dissolved in 25 ml 1 M HCl and analysed with a Perkin Elmer Optima 3000 inductively coupled plasma atomic emission spectrometer (ICP-AES). Results were checked with international and in-house standards and averaged. Spectral analysis on the V record is based on the AnalySeries program of Paillard et al. (1996) using a standard Blackman-Tukey power spectrum. Prior to analysis, data were equally spaced and detrended. A continuous wavelet transform on the V record is based on the software of Torrence and Compo (1998) and uses a Morlet mother wavelet with an order of 6.

5. Results

5.1. Depositional depth

The reconstruction of the depositional depth history of the section is based on foraminifers using percentages of planktonic foraminifers (%*P* values) and benthic foraminiferal depth markers. The relationship between %P values and depositional depth has been quantified empirically by Van der Zwaan et al. (1990) and described as depth (m) = eˆ3.587 + (0.03534*%P). The term %P refers to the number of planktonics per total number of foraminifers in splits from washed residues (using an Otto microsplitter), under the condition that splits should contain at least 100 foraminiferal specimens. The benthic foraminifers that are included in the total foraminiferal numbers consist solely of epifaunal species. The rationale of this depth equation is the notion that only a fraction of the organic carbon produced in the surface water arrives at the bottom. This fraction serves as food source for the epifaunal species and is inversely correlated with depositional depth. The number of infaunal benthic species depends on how much of the organic carbon is eventually buried in the sediments but also on the degree of oxygenation above and below the sea floor. Infaunal species are often tolerant to low oxygen conditions and their numbers thus fluctuate with in-sediment or sea floor oxygen levels rather than with depth, and for this reason these species are omitted from the %P-based depth equation. Epiphytic or other notorious shallow dwelling benthic species (see caption Table S1) are also excluded from the %*P* values, because if they occur together with upper bathyal depth markers then they should be allochthonous. The benthic foraminifers in section Agios Myron considered to be infaunal and epiphytic are listed in the caption of Table S1. Sapropel samples are excluded from the depth reconstruction because they contain abundant numbers of infaunal and rafted epiphytic specimens, and no or rare epifaunal species.

Depth estimates based on %P values show a highly fluctuating pattern especially in the cyclically-bedded unit with fluctuations as large as 800 m within two cycles (Fig. 4B and Table S1). These large fluctuations are also reflected in a SD of 54% for the average depth of the cyclically-bedded unit (364 ± 197 m). Fluctuations are smaller in the silty marls with an average depth of 141 ± 57 m. The average depth for the whole section is 293 ± 196 m.

The large and short-term fluctuations have nothing to do with changes in depth. They show that the %P method is prone to errors resulting from depositional processes, such as downslope transport and bioturbation, sampling, washing, and counting. For example, the small number of fields counted and sorting on the picking tray may be accountable for depth differences of 20–25% in three duplicate counts of silty marl samples (Table S1).

Some of the epifaunal species are to be used as depth markers (see Van Hinsbergen et al., 2005). The distribution of these depth markers in the Agios Myron section (Table S1) shows that *Uvigerina peregrina*, *Uvigerina longistriata*, *Cibicides pseudoungarianus,* and representatives of *Gyroidina* are prolific up to AM16, but become more rare and spotty above this cycle. *Uvigerina longistriata* completely disappears above AM13 and roughly the same applies for *Planulina ariminensis*. *Cibicides kullenbergi* is persistently present but rare from AM2 to AM13 and spotty above AM13. *Karreriella bradyi* instead is persistently present in the silty marls and spotty in the cyclically-bedded unit up to AM7. *Oridorsalis stellatus* is always rare and present up to the top of the section. The depth ranges for these species are given in Van Hinsbergen et al. (2005). Their distribution in the Agios Myron section shows no trends or changes: the entire succession deposited under upper bathyal conditions of 350–650 m (Fig. 4C).

Paleodepth estimates based on %*P* values and depth markers thus produce dissimilar results, whereby the %P method underestimates or the use of depth markers overestimates the depositional depth (Fig. 4B, C). Why both methods produce different results and which of the two sets of depth estimates is closest to the actual depth is unknown due to the absence of other depth markers.

5.2. The construction of the age model

5.2.1. Orbital pacing of the sedimentary cycles?

Fig. 5A shows that changes in bulk sediment Vanadium (V, ppm) concentrations closely follow the changes in lithology with high V concentrations in the sapropels. Similar patterns have been described for the cyclically-bedded sections Faneromeni on eastern Crete (Nijenhuis et al., 1996) and Gavdos (Schenau et al., 1999) and explained by the immobilization of this redox-sensitive element under reducing (anoxic) conditions (op. cit.). Spectral analysis on the V record shows that the V record and thus also the lithological record is dominated by 1.7 m, 0.99 m and 0.85 m periodicities (Fig. 5B). A continuous wavelet transform on the V record in the depth domain shows that 1.7 m, 0.99 m and 0.85 m periodicities dominate the interval of cycles AM1-15, but the 0.99–0.85 m periodicity changes to a dominant 50 cm periodicity in the interval of cycles AM16-24 (Fig. 5C). The 0.99 m and 0.85 m periodicities in the main part of the section are interpreted as being the effect of precession (23–19 kyr) on Mediterranean climate and sapropel formation as has been shown in previous studies (e.g., Hilgen et al., 1995; Lourens et al., 1996). The 1.7 m cycle can be interpreted as the effect of obliquity (41 kyr) causing a typical interference pattern of more and less distinct sapropels, i.e., higher and lower V concentrations as has been shown and modeled earlier by Lourens et al. (1996, 1998, 2001) and Bosmans et al. (2015a, 2015b). The 50 cm periodicity in the uppermost Agios Myron section is interpreted to reflect the precession cycle as well, but in this part of the section the sedimentation rate has decreased by about a factor of two.

The precession-driven origin of the sedimentary cycles is confirmed by the ash layers in section Agios Myron. The oldest and youngest one correlate with ashes 1 and 3 in section Metochia on Gavdos as is shown by the position of bioevents and the presence of amber colored sphene crystals in the Agios Myron oldest ash layer and Metochia ash 1. The ashes on Gavdos have been $^{40}Ar/^{38}Ar$ dated at 6.935 Ma for ash 1 and 6.752 Ma for ash 3 (Hilgen et al., 1997). The interval between both ash layers includes 8 cycles both in Agios Myron and Metochia so that each cycle in section Agios Myron spans 22.9 kyr corresponding with the precession frequency band.

5.2.2. The cyclostratigraphic correlation of sections Agios Myron and Metochia

Fig. 6 shows the semi-quantitative distribution of six planktonic foraminiferal species of which *Globorotalia miotumida* and *Globorotalia nicolae* are widely used for correlating Upper Miocene sediments in the Mediterranean Sea (see also Table S1). Keeled globorotaliids in the Mediterranean Upper Miocene include two different groups: an older group showing a biconvex test shape and semicircular spiral chambers

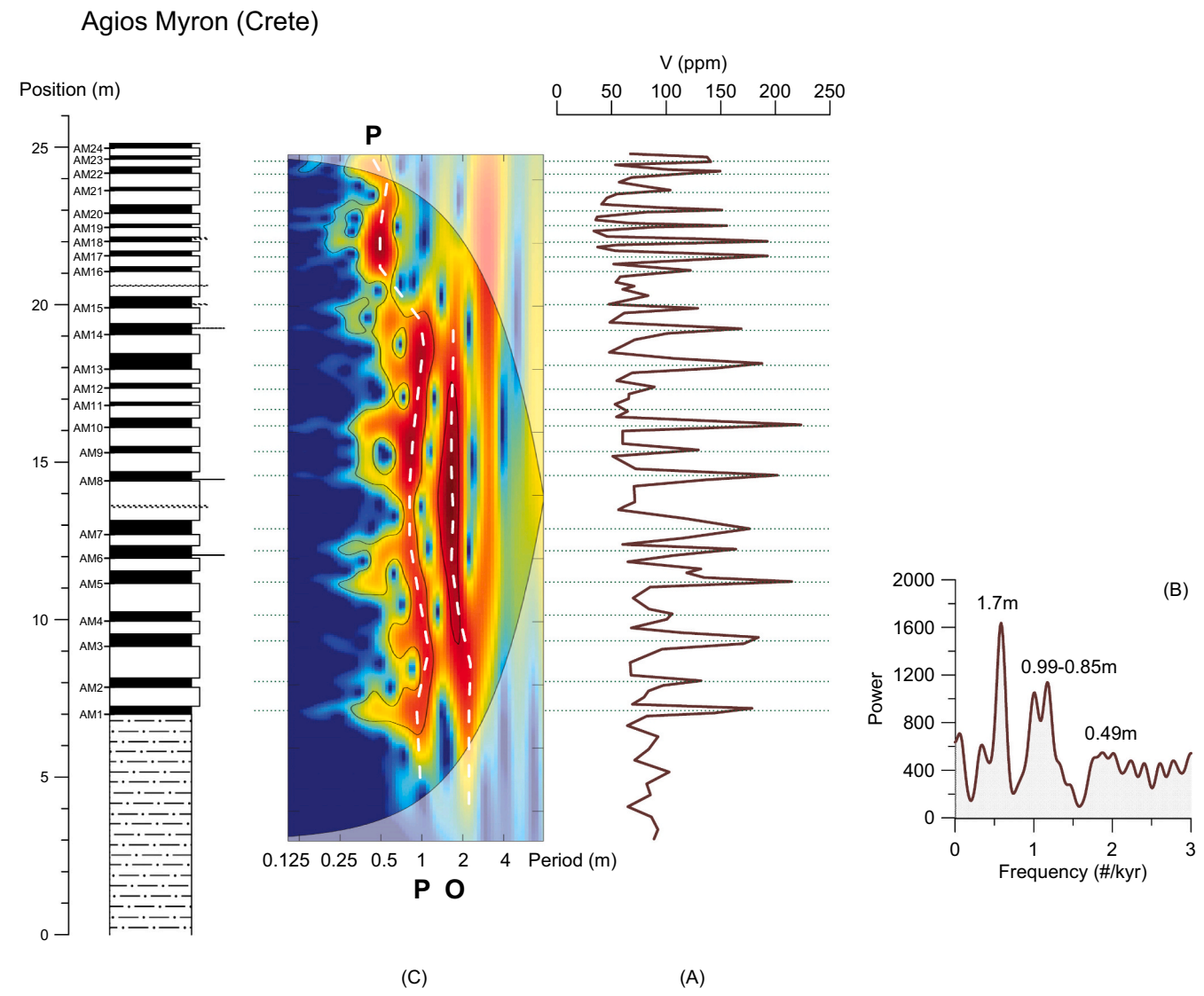

Fig. 5. Agios Myron section and Vanadium record (A) with Blackman-Tukey power spectrum (B) and Continuous Wavelet Transform (C) with P and O referring to precession and obliquity.

and a younger one characterized by a planoconvex test shape, reniform spiral chambers (Zachariasse, 1975). The older group is distinguished as *Globorotalia menardii* and includes three informal and consecutive taxonomic units, viz. *Globorotalia menardii* form 3, 4 and 5 (Tjalsma, 1971). The younger group is dominantly left coiled and replaces the dominantly right coiled *Globorotalia menardii* form 5 of the older group at the end of the Tortonian (Zachariasse, 1975; Sierro et al., 1993). In the formative years of Mediterranean biostratigraphy, various morphotypes within this younger group were described as separate species: thin and thick-shelled, high-convex types as *Globorotalia miocenica mediterranea* (Catalano and Sprovieri, 1971) and *Globorotalia saphoae* (Bizon and Bizon, 1965) and thin-shelled, low-convex types as *Globorotalia dalii* (Perconig, 1968). Later, other names were introduced but soon it became clear that the thin-shelled high and low-convex types were indistinguishable from *Globorotalia conomiozea* and *Globorotalia miotumida* respectively described by Kennett (1966) and Jenkins (1960) from the SW Pacific. The thick-shelled types have equivalents in the SW Pacific as well and were described by Walters (1965) as *Globorotalia sphericomiozea* and *Globorotalia conoidea.* Further, it became clear that the high and low-convex types in the Mediterranean Messinian, whether encrusted or not, belong to one single species for those applying an assemblage-based species concept because high and low-convex types are connected by intermediates (Zachariasse, 1979). The correct label for this group of keeled globorotallids in the Mediterranean is therefore *Globorotalia miotumida* because this name has priority. Fig. 6 shows that *Globorotalia miotumida* is present throughout the Agios Myron section indicating that the section belongs to the Messinian because in section Oued Akrech (Morocco), the First Common Occurrence (FCO) of this species coincides with the Messinian GSSP and this level is only a little older than its FO in Crete (Hilgen et al., 2000).

The unkeeled globorotaliids from the Agios Myron section belong to a phylogenetically related group of (sub)species of which *Globorotalia scitula* (described by Brady (1882) from surface sediments in the NE Atlantic) is the only living representative. In the Mediterranean, *G. scitula* is reported from throughout the Quaternary and Pliocene (e.g., Lourens et al., 1992, 1996; Rohling et al., 1993). Representatives are low-convex, small sized and dominant dextrally coiled (Zachariasse, 1975; Spaak, 1983). The subspecies *G. scitula subscitula* described by Conato (1964) from the Pliocene of northern Italy is indistinguishable from the nominate species. Rare and spotty occurrences of small-sized

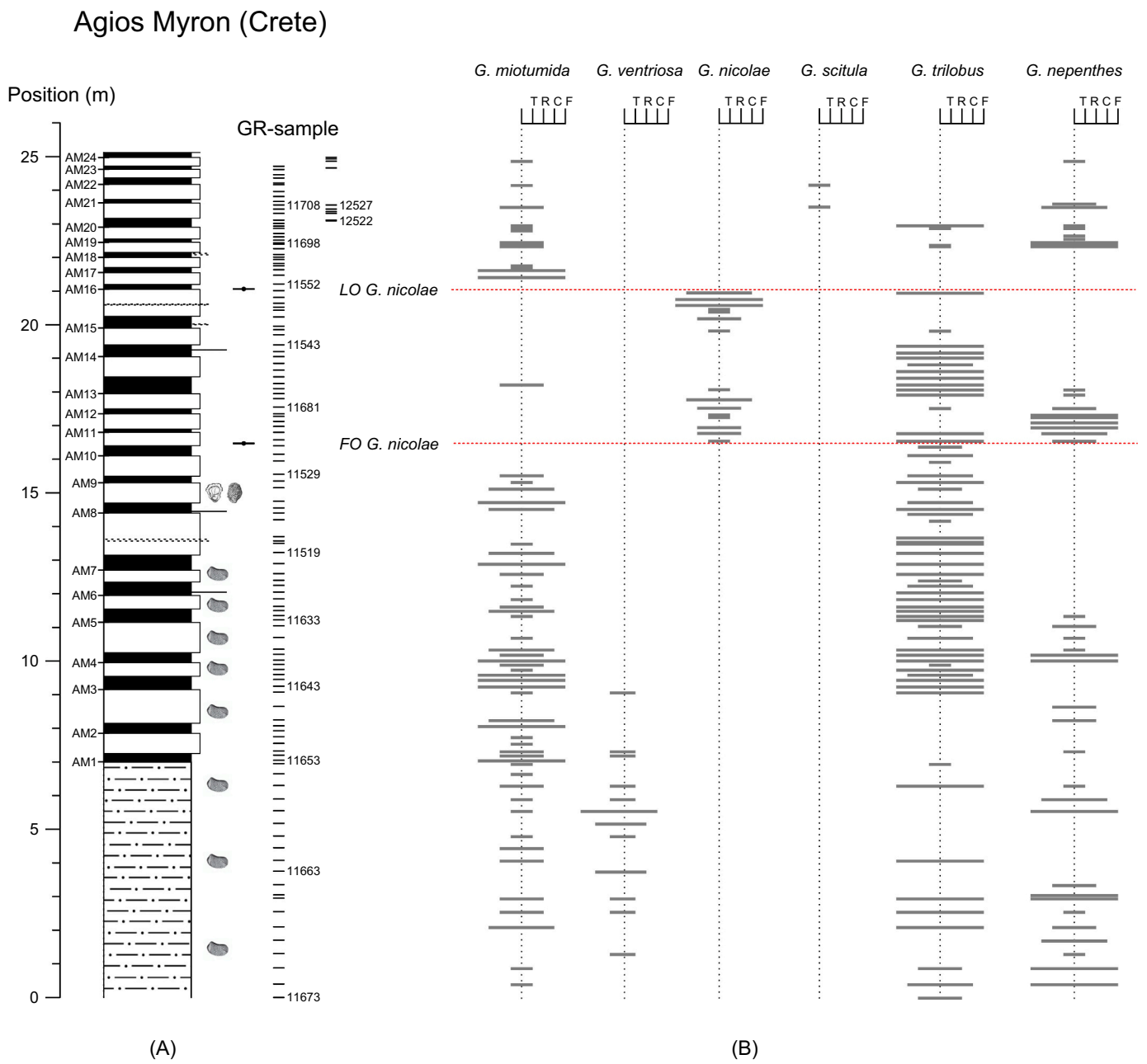

Fig. 6. The semi-quantitative distribution of six age diagnostic planktonic foraminiferal species in section Agios Myron (see Table S1 for all data).

and dextrally coiled unkeeled globorotaliids in the uppermost part of the Metochia section (unpublished data) and the Agios Myron section (Fig. 6) indicate that the stratigraphic range of the Mediterranean *G. scitula* extends down into the younger part of the pre-evaporitic Messinian. In the Agios Myron section, *G. scitula* is preceded by larger sized, low planoconvex unkeeled globorotaliids with loose coiling, inflated chambers and dominant right coiling corresponding to the description of *Globorotalia nicolae* (Catalano and Sprovieri, 1971). This species ranges from top cycle AM10 (sample Gr 11675) up into base AM16 (sample Gr 11551) and is absent in cycles AM13-14 (Fig. 6). The unkeeled globorotaliids from below the FO of *Globorotalia nicolae* are of the same size but show more compact chambers and no persistent coiling. The high-convex types, labelled *Globorotalia suterae* (Catalano and Sprovieri, 1971) in Zachariasse et al. (2011: Figs. S2 and S3), are here considered a junior synonym of *G. scitula ventriosa* (Ogniben, 1958). The low-convex form meets the description of *G. scitula gigantea* (Blow, 1959), but because both types are intergradational and thus belong to one single species, the name *Globorotalia ventriosa* has priority. Representatives of *Globorotalia ventriosa* are regularly present in the silty marls and largely absent in the interval AM1-AM10 (Fig. 6).

Two other species, *Globoturborotalita nepenthes* (Todd) and *Globigerinoides trilobus* (Reuss) show distinct absence-presence patterns within the studied interval and therefore have potential biostratigraphic value. *Globigerinoides trilobus* is almost continuously present in high numbers in cycles AM3 through AM14 and spotty below and above this interval. *Globoturborotalita nepenthes* is frequent in five short intervals: two in the silty marl unit and three in the cyclically-bedded unit.

The FO and LO of *Globorotalia nicolae* in section Agios Myron fall in the homogeneous marl of cycle AM10 and in the sapropel of cycle AM16 respectively (Fig. 6). Both bioevents are reported from the sapropels of

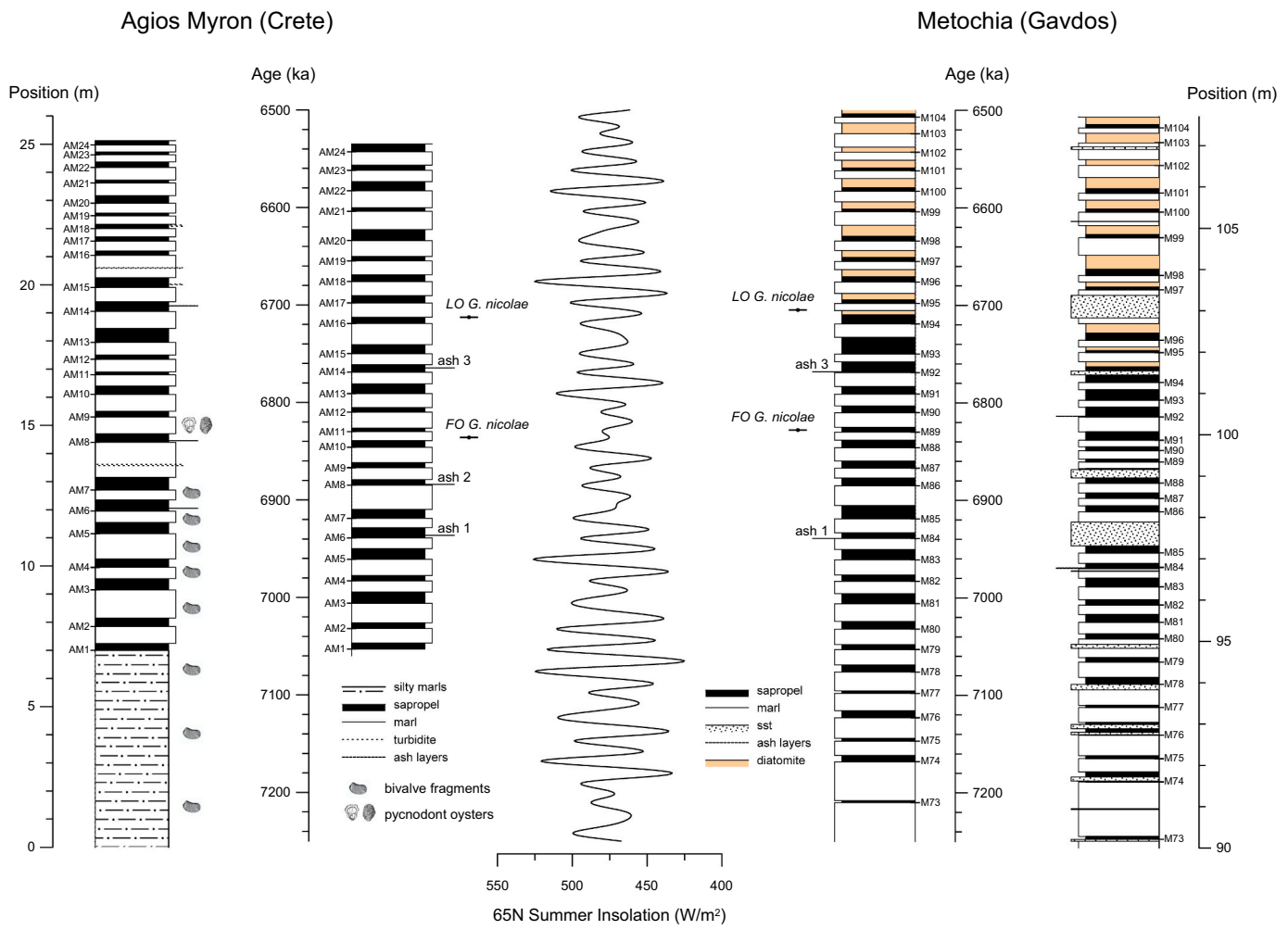

Fig. 7. Correlation of the sedimentary cycles in sections Agios Myron (central Crete) and Metochia (Gavdos). Lithology, samples and bioevents in section Metochia after Krijgsman et al. (1999). Orbitally tuned ages for base of Metochia sapropels and equivalent levels in Agios Myron are given in Table S2.

Metochia cycles M89 and M94 (Krijgsman et al., 1999) indicating that the Agios Myron cycles AM11 and AM16 equate with Metochia cycles M89 and M94 (Fig. 7). This correlation is confirmed by the presence of 4 full cycles between both bioevents and the ash layers in both sections. The ash layer in the fifth sapropel below the FO of *Globorotalia nicolae* (sapropel M89) in section Metochia (ash 1 in Hilgen et al., 1997) has an equivalent in sapropel AM6 (ash 1 in Fig. 6). Another ash layer is reported from sapropel M92, i.e., one full cycle below the LO of *Globorotalia nicolae* (ash 3 in Hilgen et al., 1997). This ash layer occurs in the time-equivalent sapropel of cycle AM14 in section Agios Myron (ash 3 in Fig. 7). The ash layer 2 in sapropel AM8 (Fig. 7) has been reported from other sections on Crete as well but is absent in section Metochia (Hilgen et al., 1997).

The above four correlation lines show that the Agios Myron cycles AM6-16 equate with Metochia cycles M84-94 (Fig. 7). If the cyclically-bedded intervals below cycle AM6 and above AM16 are without hiatuses then cycles AM1-AM5 equate with Metochia cycles M79-M83 and AM17-AM23 with M95-M102, but the lack of first order bioevents and ash layers in these intervals makes it difficult to prove this assumption. Field observations, however, suggest that we sampled an unbroken sequence (see also photograph in Figure 3B).

The Messinian in section Metochia is tuned to the La90 time series of northern summer insolation by Krijgsman et al. (1995, 1999) and Hilgen et al. (1995). In this study we tuned the Metochia section to the La2004 solutions (Laskar et al., 2004) which resulted in ages for cycles, ash layers and bioevents that may deviate only slightly from those obtained from the previous tuning. The correlation between sections Agios Myron and Metochia thus provides orbitally tuned ages for Agios Myron cycles AM1-AM24, bioevents and ash layers (Table S2).

5.3. *The planktonic foraminiferal faunas in sections Agios Myron and Metochia*

Percentages of planktonic foraminiferal taxa in the cyclically bedded unit are shown in Fig. 8 (for percent values, see Table S1). The planktonic foraminiferal fauna is dominated by the *Globigerinoides obliquus* group [including *Globigerinoides obliquus* Bolli and *Globoturborotalita apertura* (Cushman)], *Globigerina bulloides* group [including *G. bulloides* d'Orbigny and *Globigerina pseudobesa* (Salvatorini)] and *Neogloboquadrina acostaensis* (Fig. 8). Species that are less continuously present and in smaller percentages are *Globigerinita glutinata* (Egger), *Turborotalita quinqueloba* Natland, *Orbulina universa* d'Orbigny, *Globigerinella siphonifera* (d'Orbigny), and globorotaliids. Neogloboquadrinids are dominantly left coiled in agreement with their coiling change from left to right at a much younger level in the pre-evaporitic Messinian as first reported by Zachariasse (1975) and first dated at 6.337 Ma by Hilgen and Krijgsman (1999). Fig. 8 also shows that the patterns of *Globoturborotalita nepenthes* and *Globigerinoides trilobus* correspond well to those in Fig. 6 though their numbers in the total counts are small.

The planktonic foraminifers from the M79-M102 interval in section Metochia have been counted in the same way and on the same taxa as we did for the Agios Myron section (see Fig. 9 and Table S3).

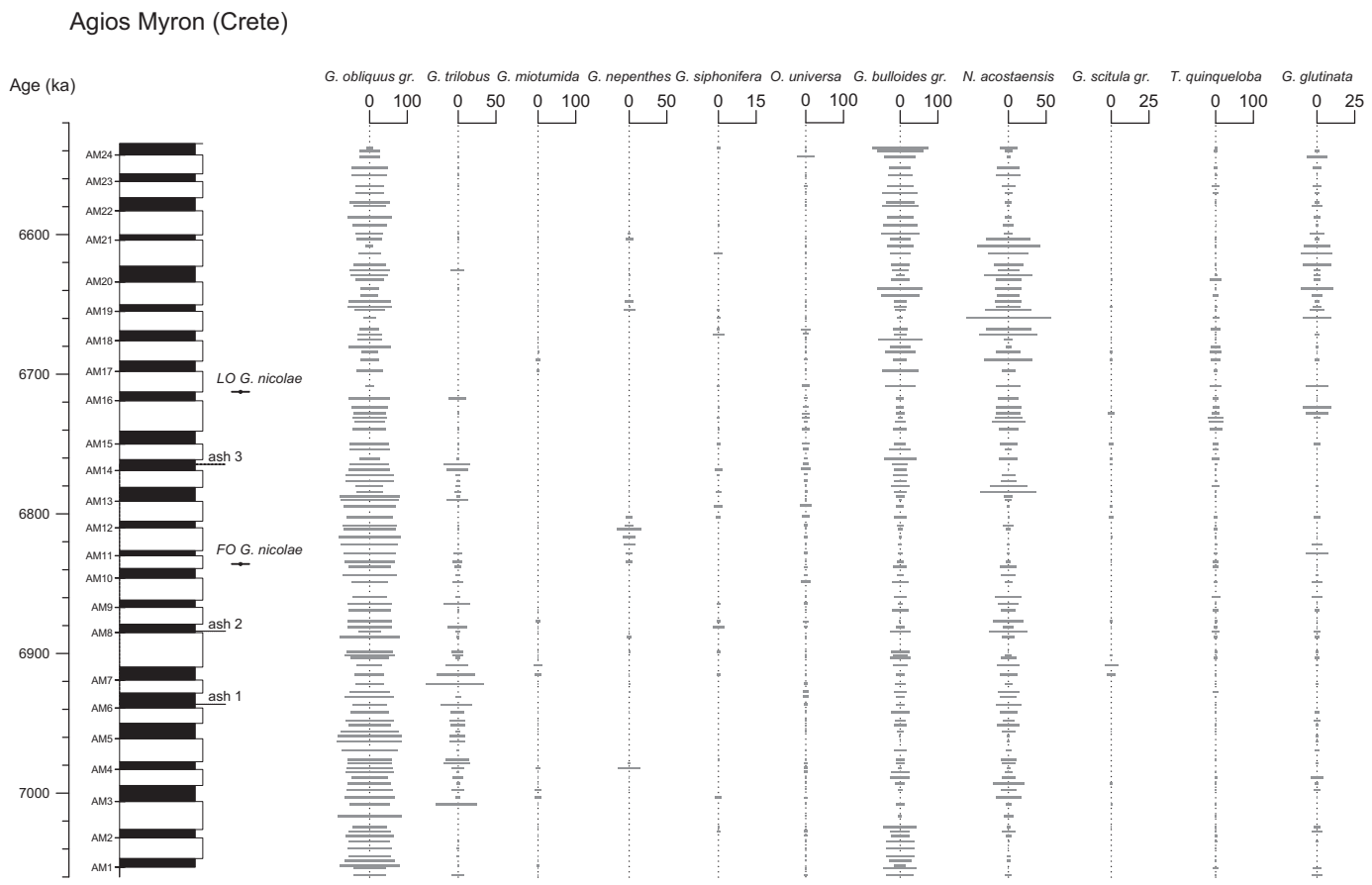

Fig. 8. Percentages of planktonic foraminiferal taxa in section Agios Myron (see Table S1 for all data).

5.4. Foraminiferal oxygen and carbon isotope data from Agios Myron

Stable oxygen and carbon isotopes were measured in planktonic and benthic foraminifers from 98 homogeneous and laminated marl samples from the cyclically-bedded unit in the Agios Myron section. Measured planktonic foraminifers are specimens of the surface dwelling *Globigerinoides obliquus,* whereas the benthic foraminifers belong to the group of *Cibicides (pseudo)ungarianus* with some specimens close to *Cibicides kullenbergi.* All isotope data are tabulated in Table S1 and plotted versus lithology and in the time domain in Fig. 10. This figure shows that variations in planktonic oxygen isotope values correlate to the cyclically changes in lithology with most depleted values occurring in sapropels. Bundles of maximum negative planktonic oxygen isotope values are concentrated in the upper and lower part of the section and reflect modulations of the 400 and 100 kyr eccentricity cycle on climate precession (see northern summer insolation record in Fig. 7). No correlation to lithology is shown for the planktonic carbon isotope and benthic oxygen isotope values (Fig. 10).

6. Discussion

6.1. On the sudden appearance of sapropels in section Agios Myron

The distribution and water depths of sapropels S1 and S5 suggest that the Upper Depth Limit (UDL) for Late Quaternary sapropel formation in the open eastern Mediterranean is ~300 m (Rohling and Gieskes, 1989). The sudden appearance of sapropel AM1 at 7.05 Ma (Fig. 7) therefore suggest that the Agios Myron site deepened from above to below the UDL for Messinian sapropel formation. If we combine the depth data obtained from the %*P* values and presence of depth markers, then the depositional depth may have changed from 200 to 350 m before to 350–560 m after 7.05 Ma, suggesting that the Messinian UDL for sapropel formation at the Agios Myron site was not so much different from today's UDL. Above depth ranges are based on %P maximum and depth marker minimum depth estimates (see Fig. 4B,C).

However, the above conclusion is only valid if we can exclude the presence of a hiatus at the base of sapropel AM1. Since hiatuses in deep marine sediments are generally difficult to identify in outcrop, we compare the Agios Myron section with seven other Messinian sections in the NW Heraklion Basin (see Fig. 2 for location and Fig. 11 for lithology). Just as in the Agios Myron section, sedimentation at these sites begins with fluvial to inner-shelf clastic or biogenic sediments which pass upwards into outer shelf to upper bathyal silty marls without sapropels and then into upper bathyal marls with sapropels (Fig. 11). Section 1 shows that the Tortonian-Messinian boundary falls in the silty marl unit without sapropels. This boundary equates with the base of Metochia cycle M73 (Hilgen et al., 2000). Exposed contacts between the fluvial-neritic unit and the upper bathyal silty marls without sapropels are sharp and because of absence of evidence for an unconformity, interpreted to reflect rapid deepening of the basin. Plankton foraminiferal biostratigraphy and ash layers show that the basal sapropel in six sections is younger than in section Agios Myron. Only the basal sapropel in section 6 seems to be time-equivalent with the one in Agios Myron (Fig. 11).

The silty marls without sapropels are thus in six out of eight sections separated from the overlying cyclically marl unit by hiatuses spanning different lengths of time. In section 5, even the entire silty marl unit is removed. In view of the upper bathyal depositional environment for the cyclically-bedded unit, hiatus formation should have been caused by submarine sliding, with the note that sliding happened at different times. Most sections even show multiple submarine sliding events (Fig. 11). Submarine sliding likely resulted from *syn*-depositional tilting

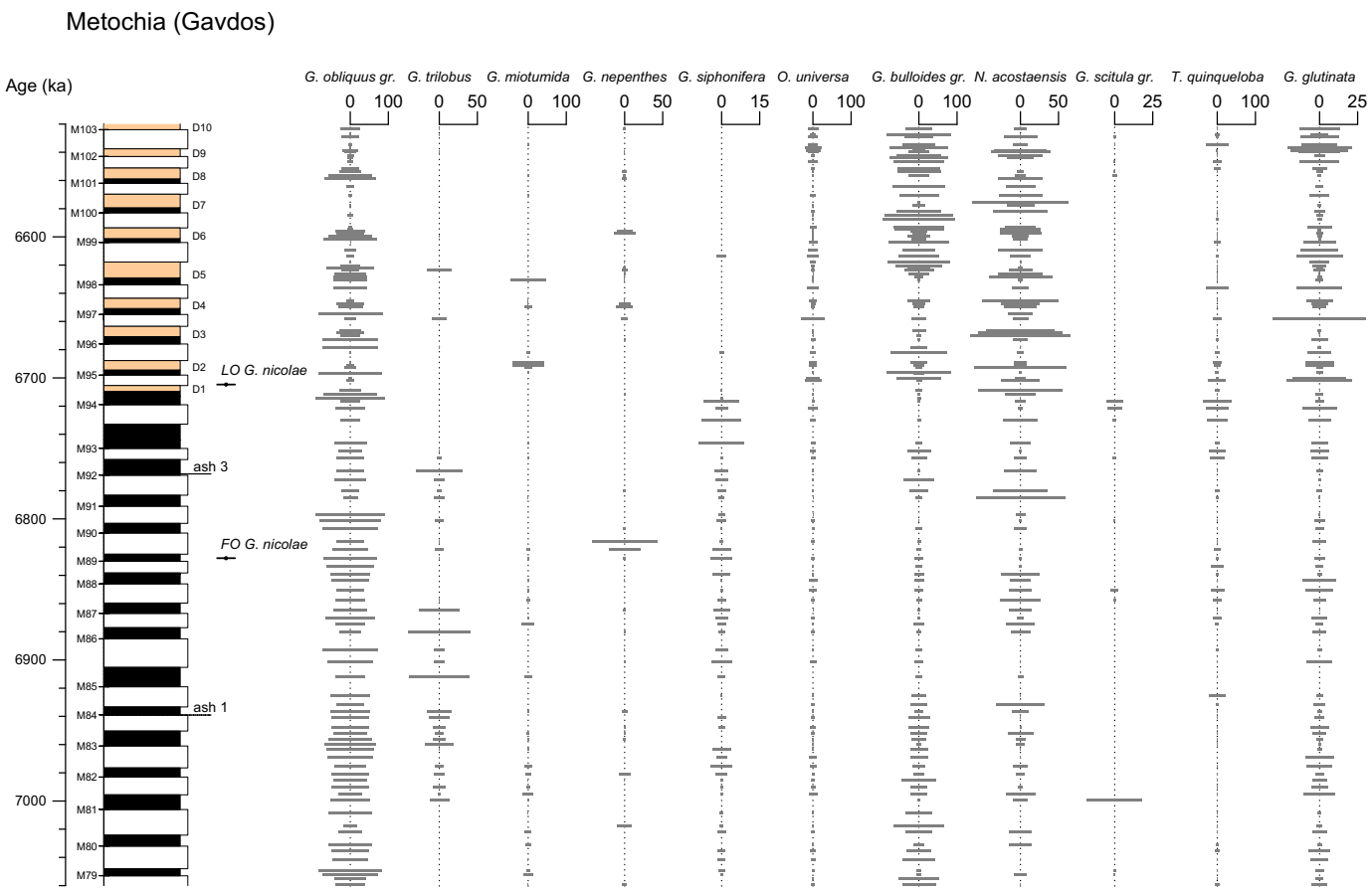

Fig. 9. Percentages of planktonic foraminiferal taxa in the interval of cycles M79-M102 in section Metochia (see Table S3 for all data).

of hanging wall blocks and/or seismic activity. The fact that the basal sapropel in section 6 seems time-equivalent with the basal sapropel in the Agios Myron section, whereas the basal sapropels in the other sections are significantly younger suggests a conformable contact between the silty marl unit and the cyclically bedded marl unit in section Agios Myron. The section remains complete up to cycle AM24, but then becomes disturbed possibly by syn-depositional sliding and post-depositional mass wasting in the Early Pliocene (see Fig. 3C).

The depositional depth history of the Agios Myron Formation thus consists of three steps. A first step marks the beginning of subsidence of the northern Heraklion Basin after more than 2 million of years of subaerial erosion. In a second step the basin subsides abruptly to outer shelf - upper bathyal depths, whereas in a third step the basin deepens to below the UDL of Messinian sapropel formation.

6.2. *The planktonic foraminiferal change at 6.72 Ma*

The planktonic foraminiferal faunas from Agios Myron and Metochia sections change around 6.72 Ma and that change manifests itself most clearly in the increase of the *G. bulloides* group and decrease of the *Globigerinoides obliquus* group (see Figs. 8 and 9). The overturn in these two most abundant shallow dwelling species groups shows up as well in the results of the principal component analysis (PCA) on the data from both sections. The first principal component (PCA1) discriminates between the *G. bulloides* group and *Globigerinoides obliquus* group (see Table S4 for species loadings) and the scores clearly show a shift to more positive values and – especially in Metochia – greater variability after 6.72 Ma (Fig. 12). PCA2 discriminates between neogloboquadrinids and the groups of *G. bulloides* and *Globigerinoides obliquus* (Table S4). The PCA2 scores show greater variability after 6.72 Ma with peak occurrences of neogloboquadrinids (maximum positive scores) in the diatomites on Gavdos (Fig. 12 and Table S5). Such peaks do not systematically occur in the post-6.72 Ma sapropels of section Agios Myron (Fig. 12). Average percent values of neogloboquadrinids are higher in both sections after 6.72 Ma than before and that applies both for laminated and homogeneous marls (Table S5).

The most obvious explanation for the higher positive PCA1 scores after 6.72 Ma is that overall conditions became more eutrophic because the shallow-dwelling, symbiont-barren *G. bulloides* is often specified in these terms (e.g., Prell and Curry, 1981; Zhang, 1985; Jonkers and Kučera, 2015). In the Mediterranean, this species flourishes in the winter with decreasing abundance from the more eutrophic western to the oligotrophic eastern Mediterranean (Pujol and Vergnaud Grazzini, 1995) and is extremely rare in the ultra-oligotrophic southeastern Levantine Basin (Avnaim-Katav et al., 2020).

The greater abundance of the *G. bulloides* group in the post-6.72 Ma sediments in both sections thus seems to indicate that this part of the eastern Mediterranean became more eutrophic after 6.72 Ma. Neogloboquadrinids predominantly dwell subsurface in low latitude regions with a shallow and steep pycnocline and a well-developed deep chlorophyl maximum (DCM) layer (e.g., Fairbanks and Wiebe, 1980; Fairbanks et al., 1982; Rohling and Gieskes, 1989). Their higher average percentages in the post-6.72 Ma sediments of both sections (Table S5) therefore point to an overall better developed DCM and thus to higher productivity. The DCM seems particularly well-developed during periods of diatomite formation on Gavdos because such periods are characterized by peak occurrences of neogloboquadrinids (Fig. 12) and by the presence of diatom species having their habitat in the nutricline (Pérez-Folgado et al., 2003).

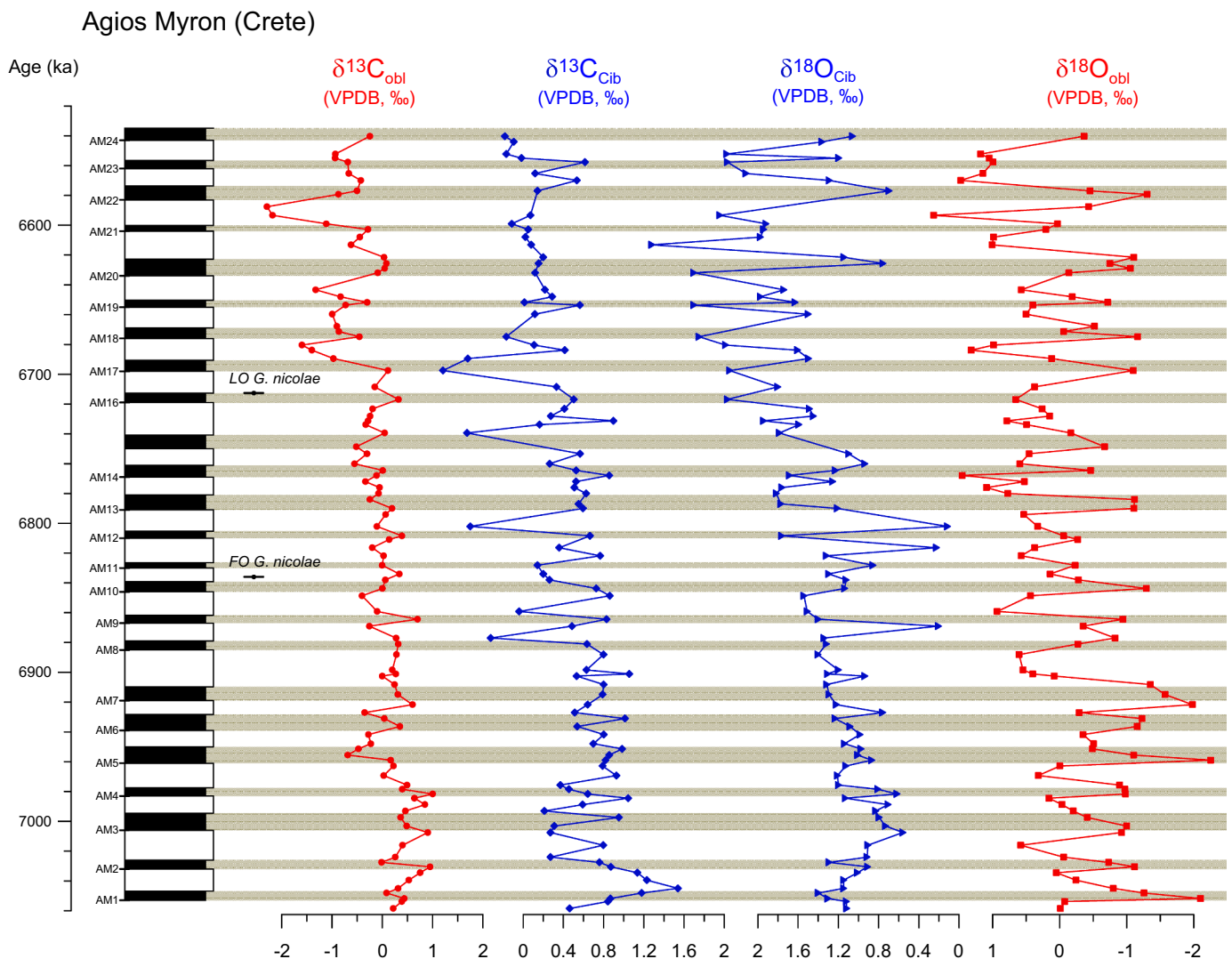

Fig. 10. Oxygen and carbon isotope curves for section Agios Myron based on measuring *Globigerinoides obliquus* and *Cibicides (pseudo)ungarianus* in ninety-eight samples from sapropels and homogeneous marls.

6.3. The change in benthic foraminiferal oxygen isotopes at 6.74 Ma

The close correlation between depleted planktonic oxygen isotope values and laminated marls in the Messinian at Agios Myron on central Crete (Fig. 10) has also been reported from similarly cyclically-bedded Upper Miocene sections on eastern Crete (Nijenhuis et al., 1996), Gavdos (Schenau et al., 1999) and SE Spain (Sierro et al., 2003) and attributed to the wet climatic conditions at times of minimum precession (op. cit.; for an overview of sapropel formation and climatic conditions, see Rohling et al., 2015). The deep-water benthic oxygen isotope record is not correlated to lithology (Fig. 10). In Fig. 13 we removed the effect of precession-controlled fluctuations in freshwater input on the isotope composition by plotting only the planktonic and benthic values from the homogeneous marls in order to better visualize any longer-term changes. One such a change is visible around 6.74 Ma and corresponds with a shift to heavier values in the deep-water benthic oxygen isotopes (Fig. 13). Averaging benthic oxygen isotope values from below and above the 6.74 Ma level shows that the enrichment is 0.7‰ (Fig. 13).

In the absence of published evidence for circum-Mediterranean climate cooling around this time, we interpret the enrichment in benthic oxygen isotopes around 6.74 Ma in terms of an increase in deep water salinity. This salinity increase at 6.74 Ma appears to be Mediterranean-wide given published benthic oxygen isotope enrichments around this time from northern Italy (Kouwenhoven et al., 1999) and southeastern Spain (Sierro et al., 2003) and therefore should be attributed to diminished outflow of Mediterranean water. If we apply the equations between the oxygen isotope composition and salinity of Mediterranean seawater of Pierre (1999) and Cox et al. (2011) then the enrichment of 0.7‰ around 6.74 Ma corresponds to a salinity increase of 2.9 ± 0.3‰ for the deep water.

Since the enrichment in the benthic oxygen isotopes of section Agios Myron occurred in a period of low-amplitude glacial cycles (Hodell et al., 2001; Drury et al., 2018), the restriction in the gateway area and corresponding reduction in Mediterranean outflow should be imposed by tectonic shallowing/narrowing of the Gibraltar gateway rather than by glacio-eustasy [for an overview of the Late Miocene paleogeographic evolution of the Gibraltar area, see Sissingh, 2008 and Krijgsman et al., 2018]. Reducing the salty outflow will lead to a correspondingly smaller inflow of normal saline Atlantic surface water provided that the net flux of evaporation, precipitation and river discharge remains the same to conserve salt and volume. As a consequence, both the residence time of Mediterranean water and the salinity of the surface water should increase as well. Evidence for an increase in residence time is shown by the 0.4‰ depletion of the average benthic carbon isotope value above the 6.74 Ma level (Fig. 13). However, the predicted salinity increase of the

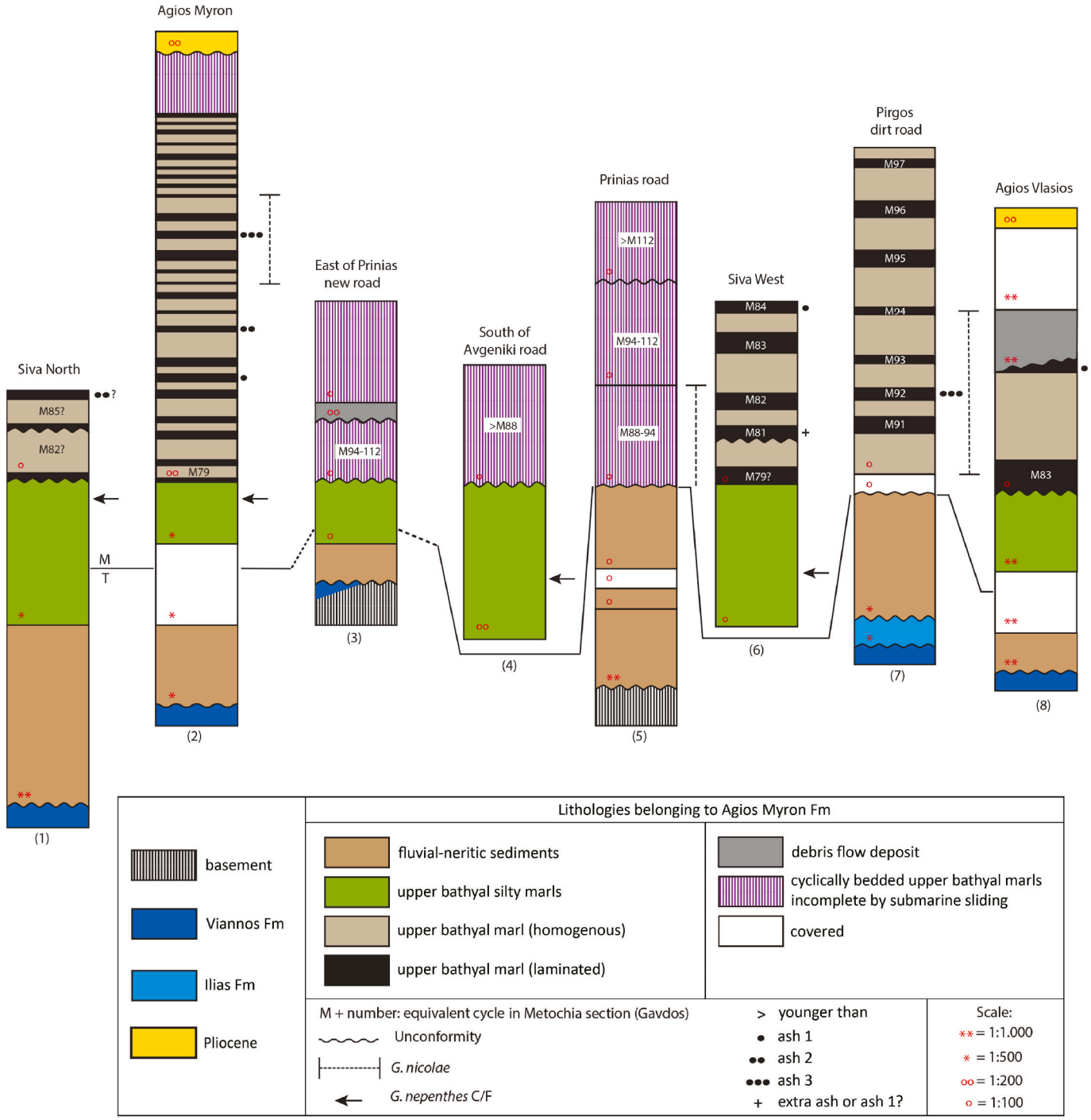

Fig. 11. Lithology and depositional conditions of eight sections belonging to the Agios Myron Fm in the NW Heraklion Basin. Location of sections is given in Fig. 2 except section 8 which is located some 9 km to the NE of Dafnes. M: Messinian; T: Tortonian.

surface water is not really shown by the planktonic oxygen isotope values though the average value is 0.5‰ heavier above the 6.74 Ma level than below (Fig. 13). Fluctuations in planktonic oxygen isotopes, however, are great even after removing the laminated marl samples and still seem to preserve the effect of 400 and 100 kyr eccentricity cycles on precession (discussed in 5.4), probably through bioturbation, whereby *Globigerinoides obliquus* from the sapropels below is mixed upwards into the overlying homogeneous marls.

Fig. 13 further shows that the difference between the average planktonic and benthic oxygen isotope values from before and after 6.74 Ma remains at 1.2 ± 0.1‰. This difference is interpreted as a surface to deep water T-difference of 5.3 ± 0.9 °C (using paleotemperature equations of Shackleton (1974) and Bemis et al., 1998) which is not unrealistic given the upper bathyal depositional depth for the Agios Myron section and comparable with the modern T-gradient for the eastern Mediterranean of 6–6.5 °C (Kassis and Korres, 2020).

The summary conclusion of the above discussion is that there is isotope evidence for an increase in salinity around 6.74 Ma, but further underpinning should come from additional isotope and biomarker studies on time-equivalent sections preferably across a large paleodepth gradient to learn more about the (sub)surface salinity layering in the pre-evaporitic Messinian Mediterranean.

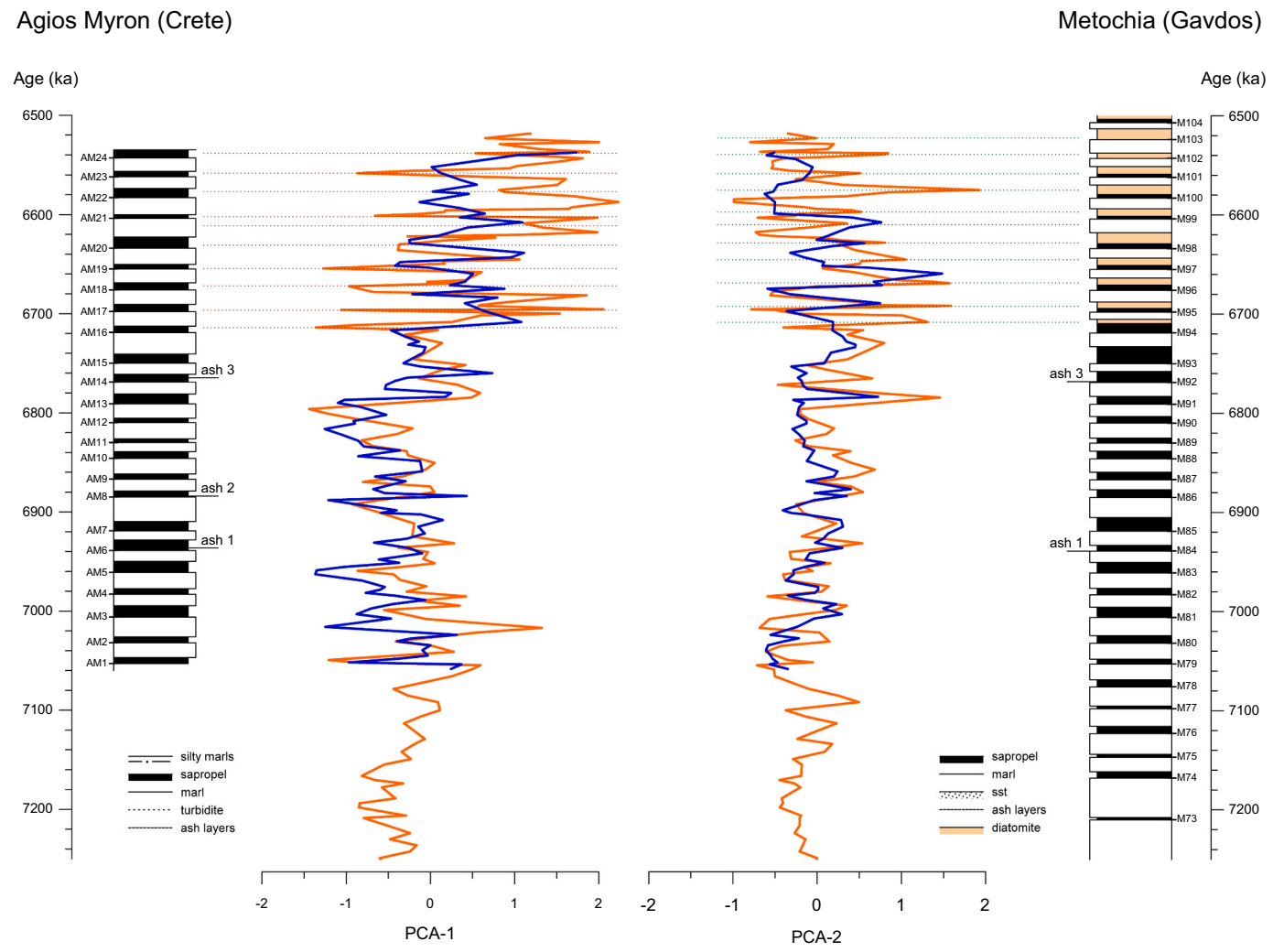

Fig. 12. PCA-1 and PCA-2 scores for the planktonic faunas in sections Agios Myron and Metochia. PCA-1 and PCA-2 represent 58% and 22% of the total variance. Species loadings are given in Table S4.

6.4. On the origin of the eutrophication after 6.72 Ma

Earlier (in chapter 6.2), we concluded that the change in the planktonic foraminiferal faunas in sections Agios Myron and Metochia at 6.72 Ma points to eutrophication and it is logically to relate eutrophication to the isotope-based evidence for a salinity increase 20 kyr earlier at 6.74 Ma (see chapter 6.3). In the simplest scenario, the salinity increased mainly in the deep water allowing the pycnocline/nutricline to occupy an overall shallower position causing a correspondingly better developed DCM, because the DCM can only develop when the base of the euphotic zone is within the pycnocline/nutricline (Rohling and Gieskes, 1989). However, this scenario is not supported by the same difference of 1.2 ± 0.1‰ between average planktonic and benthic oxygen isotope values below and above the 6.74 Ma level though averages above the 6.74 Ma level are heavier (Fig. 13 and chapter 6.3). The eutrophication at 6.72 Ma thus requires a scenario based on an overall salinity increase at 6.74 Ma and is illustrated in Fig. 14.

Periods of laminated marl formation are characterized by excess runoff and precipitation resulting in the formation of less dense subsurface (intermediate) water and correspondingly shallower position of the pycnocline/nutricline: conditions favorable for DCM development (see e.g., Rohling and Gieskes, 1989). Trophic conditions for the average laminated marl bed before and after 6.72 Ma are comparable with regard to the input of riverborne nutrients, but differ after 6.72 Ma in the (intermittent) entrainment of more nutrient-rich subsurface water into the photic zone through winter mixing possibly resulting in more intense algal blooms and increased abundance of the *Globigerina bulloides* group. After becoming stably stratified in early spring, the nutrient enriched mixed layer develops a more expanded DCM (Figs. 14a-b) with correspondingly greater abundances of neogloboquadrinids (Figs. 8 and 9; Table S5). The reason for the nutrient enrichment of the subsurface water is the increased residence time of Mediterranean water after 6.74 Ma.

Periods of homogeneous marl deposition are – in contrast to periods of laminated marl formation (see above) – characterized by 1) a deeper position of the pycnocline due to absence of positive buoyancy input (Rohling and Gieskes, 1989), and 2) late winter storms of southerly origin scattering Saharan dust (including nutrients) over the eastern Mediterranean (Lourens et al., 2001; De Boer et al., 2021). Increased southerly winter storms over the eastern Mediterranean at times of maximum precession (and homogeneous marl deposition) is also the outcome of a climate modeling study on the sources of precipitation over the Mediterranean at times of minimum precession by Bosmans et al. (2020). There is no reason to assume that frequency and intensity of these southerly winter storms at times of maximum precession (and homogeneous marl deposition) has changed after 6.72 Ma, but the residence time did because it increased. Consequently, deep winter mixing entrains more nutrient-rich subsurface water into the photic zone causing a better developed DCM in early spring with increased abundance of the *G. bulloides* group and neogloboquadrinids in the

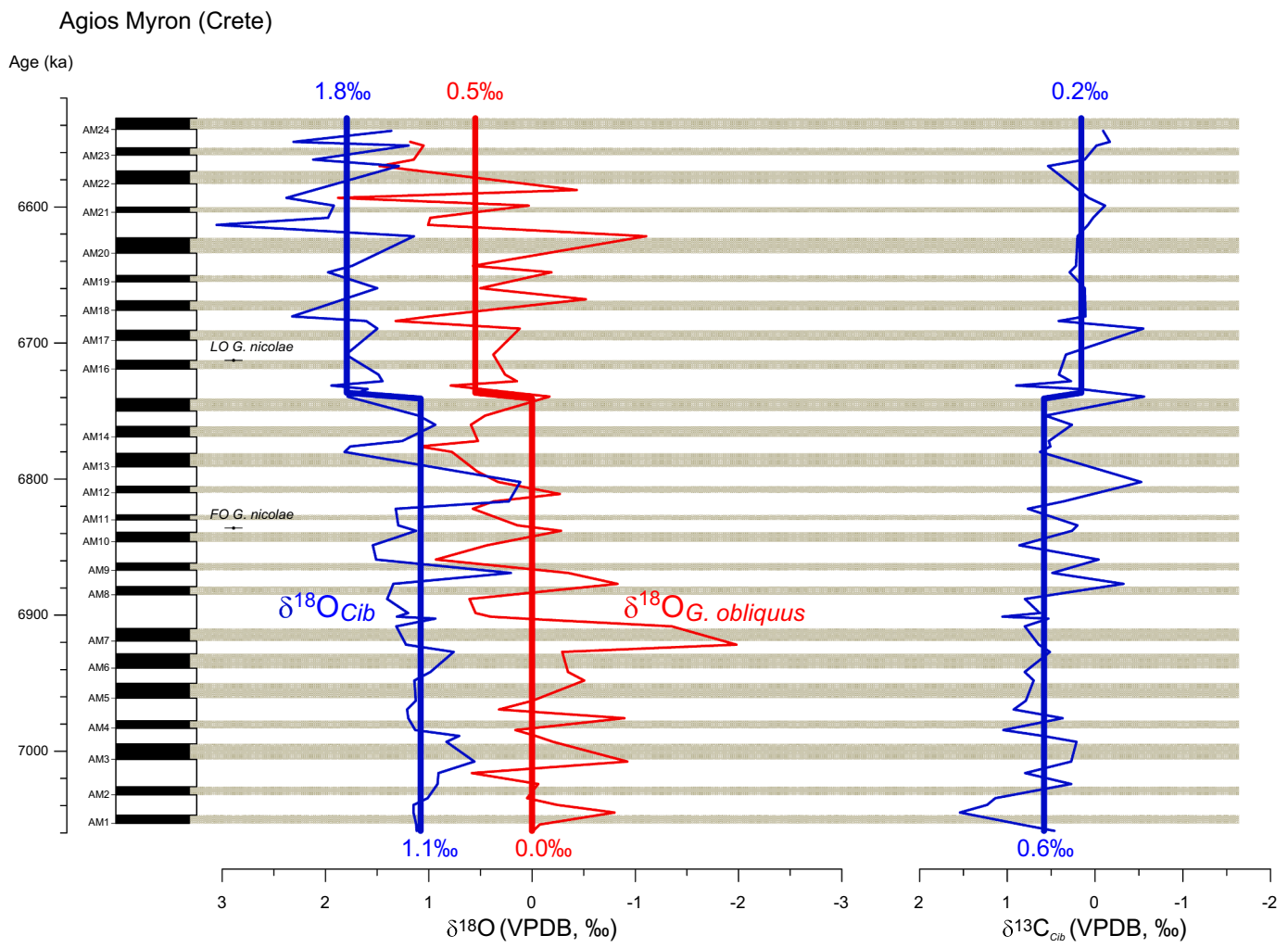

Fig. 13. Stable isotope curves for *Globigerinoides obliquus* (oxygen isotopes) and *Cibicides (pseudo)ungarianus* (oxygen and carbon isotopes) for homogeneous marls only. Solid lines represent average values before and after 6.74 Ma.

average homogeneous marl bed after 6.72 Ma (Table S5 and Figs. 14c-d). Winter mixing and dust (nutrient) input is invoked by Pérez-Folgado et al. (2003) as well to explain the greater abundance of *G. bulloides* in the homogeneous marls of four diatomite cycles on Gavdos Island.

6.5. *On the origin of diatomites on Gavdos and their absence at Agios Myron*

The one-to-one correlation of the cycles in sections Agios Myron and Metochia shows that in the post-6.72 Ma cycles on Gavdos, sapropels and homogeneous marls are separated by diatomite layers but that does not apply for the time-equivalent cycles of the 100 km more northerly located Agios Myron site on central Crete (Fig. 7). Why diatomites occur on Gavdos and not on central Crete will be discussed below.

We concluded earlier (in chapter 6.4) that conditions during the deposition of the average laminated marl bed after 6.72 Ma were more eutrophic than before because of a more expanded DCM in late winter-early spring both on Gavdos and at Agios Myron (Fig. 14a-b). These grossly similar average trophic conditions break down in periods of diatomite formation. Such periods whereby precession changes from minimum to maximum values are characterized by a much greater abundance of neogloboquadrinids on Gavdos than at Agios Myron (Table S5) pointing to a much better developed DCM on Gavdos than at the same time at Agios Myron.

A possible reason for the greater DCM productivity on Gavdos is that winter storm activity may have increased already at the transition from minimum to maximum precession. This situation has not been modeled by Bosman et al. (2020) (as it was for periods of maximum precession, see in 6.4), but if it were true then it should also apply for such transitions before 6.72 Ma. If the activity of southerly winter storms and associated cyclonic wind fields indeed increased already at the transition from minimum to maximum precession, then it may have caused divergent conditions at the open marine Gavdos site, but not at the Agios Myron site which was at that time sandwiched between mountain blocks (Van Hinsbergen and Meulenkamp, 2006; Zachariasse et al., 2011). Consequently, divergence may have tilted the shallow pycnocline/nutricline into the photic zone thereby extending the seasonal DCM from winter into spring after 6.72 Ma resulting in the formation of diatomites on Gavdos (see Fig. 14e).

Apart from Gavdos, Messinian diatomites are also known from other areas in the Mediterranean. Their distribution and origin is recently reviewed by Pellegrino et al. (2018, 2020) and makes clear that there are currently different explanations for Messinian diatomite formation. The one closest to our model is that of Filippelli et al. (2003) for time-equivalent diatomites in SE Spain. This model evokes subsurface nutrient buildup and sapropel formation at times of minimum precession and nutrient recycling under divergent conditions at times of maximum precession with diatomite formation in the initial phase.

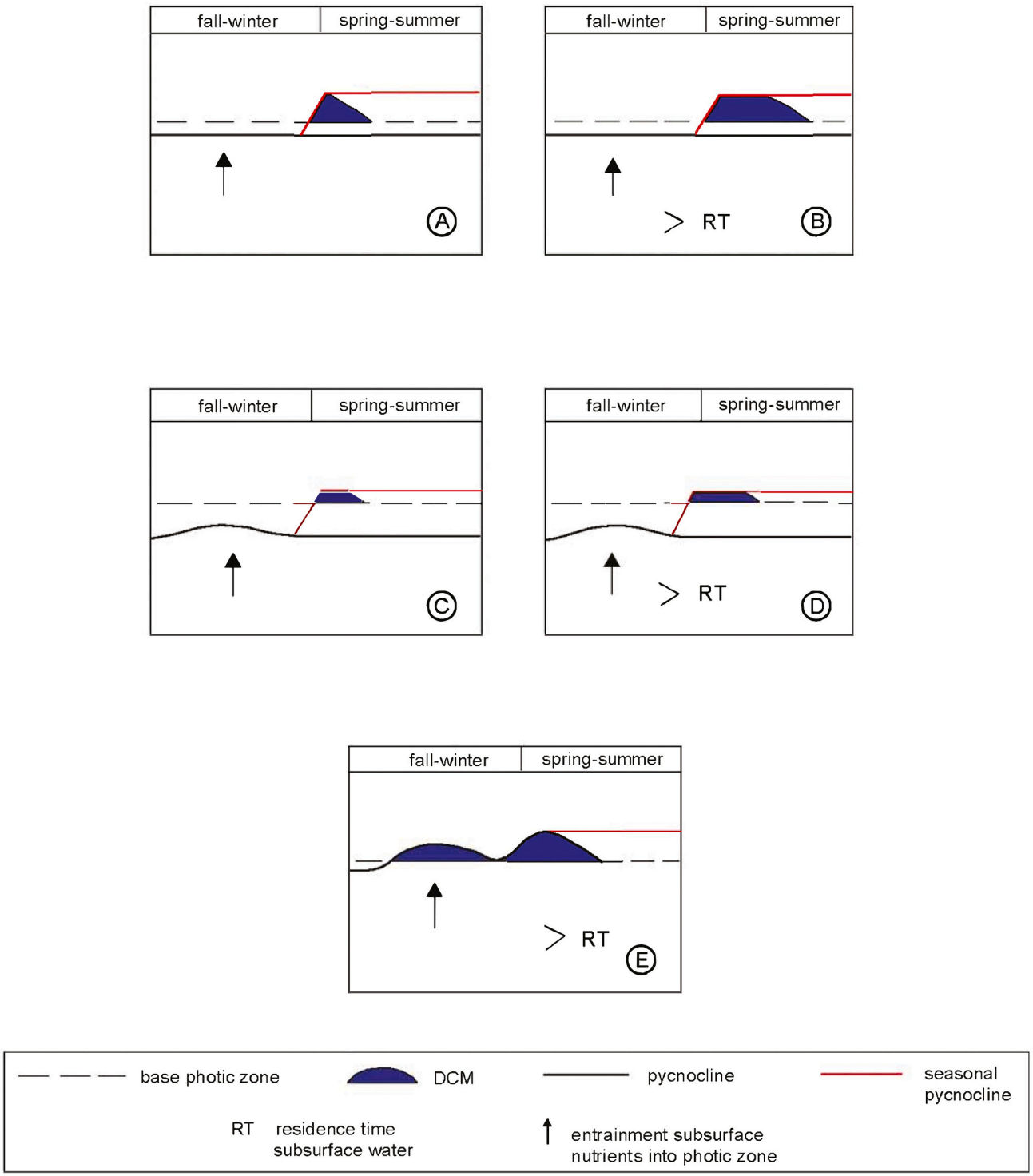

Fig. 14. Portrayal of the trophic conditions for the average laminated marl before and after 6.72 Ma (A and B), idem for the average homogeneous marl and the effect of a divergence on pycnocline for the Gavdos site (C and D), and idem for the average diatomite on Gavdos (E). Inferred conditions are based on the planktonic foraminiferal faunas at both sites and stable isotope data from Agios Myron, and explained in the text.

6.6. A role for silica preservation?

The onset of diatomite formation on Gavdos is accompanied by the sudden and massive presence of diatoms, radiolarians and silicoflagellates and at about the same time by spicules of bottom dwelling siliceous sponges. Especially the occurrence of siliceous sponge spicules in Metochia and their absence in Agios Myron suggests an additional role for silica preservation in the formation of diatomites on Gavdos and if true then it should have played out through a difference in depositional depth between both sites.

The depth for the Metochia section below the diatomite interval is estimated at 1200 m by Van Hinsbergen and Meulenkamp (2006) using %*P* values. A depth range of roughly 750–1000 m can be concluded from the distribution of benthic foraminiferal depth marker species in Seidenkrantz et al. (2000) and their depth ranges given in Van Hinsbergen et al. (2005). Depth estimates become unreliable for the interval with

diatomites because of the less diversified foraminiferal (planktonic and benthic) faunas and the vanishing of depth marker species, but the lithology does not provide any evidence for shallowing. The estimated depositional depth of 364 ± 197 m using %P values and 350–650 m using depth markers for the cyclically-bedded part of section Agios Myron (cycles AM1-24) is thus substantially less than the depth of around 1000 m for the time-equivalent part on Gavdos. The suggestion we make here is that the 1000 m deep and perhaps stagnant bottom water at the Gavdos site could have preserved the siliceous microfossils better than on the 500 m shallower and possibly better ventilated sea floor at Agios Myron.

7. Conclusions

The Agios Myron section is located on a fault block that begins to subside in the latest Tortonian and (based on the sudden appearance of sapropels) passed the upper depth limit for sapropel formation at 7.05 Ma. Depositional depth estimates suggest that the Messinian upper depth limit for sapropel formation at Agios Myron was probably not so much different from the 300 m for Late Quaternary sapropel formation in the open eastern Mediterranean.

The post-7.05 Ma sapropels are part of a cyclically bedded unit of 24 cycles with sapropel at bottom and homogeneous marl at top. Correlation of these cycles to those in the orbitally tuned Metochia section on Gavdos provides tuned ages to section Agios Myron and shows that the upper 9 sapropels at Agios Myron equate with sapropel-diatomite couplets on Gavdos.

The increase in abundance of the *G. bulloides* group and neogloboquadrinids at 6.72 Ma is interpreted in terms of eutrophication and related to isotope-based evidence for an increase in salinity 20 kyr earlier at 6.74 Ma. The onset of diatomite formation on Gavdos at 6.72 Ma thus coincides with overall eutrophication, but peak occurrences of neogloboquadrinids in the Gavdos diatomites and the absence of such peaks in time-equivalent levels at Agios Myron suggest that geographic differences in DCM productivity resulted in diatomite formation on Gavdos and not at Agios Myron. As a possible explanation for this dichotomy in DCM productivity we invoke geographic differences in divergent conditions imposed by increased winter storm activity at transitions from minimum to maximum precession. We further suggest that the preservation potential for siliceous microfossils has been greater for the 1000 m deep Gavdos site than for the shallower (500 m) and better ventilated Agios Myron site.

Data availability

The data associated with this article can be found in Supplementary material.

Declaration of Competing Interest

The authors declare no conflict of interest.

Acknowledgements

Arnoud Kerklaan is acknowledged for the ICP-AES analysis on bulk sediment samples. Arnold van Dijk is thanked for measuring the isotope samples and Cindy Schrader for weighing the samples. Paul Meijer is acknowledged for sharing his expertise on the Messinian Mediterranean. Comments by Hugo Corbi, Thomas J. Algeo, and one anonymous reviewer were of great help in improving our manuscript. This research was carried out under the program of the Netherlands Earth System Science Centre (NESSC), financially supported by the Dutch Ministry of Education, Culture and Science (OCW).

Appendix A. Supplementary data

Supplementary data to this article can be found online at https://doi.org/10.1016/j.palaeo.2021.110633.

References

Angelier, J., 1975. Sur l'analyse des phases superposées de la tectonique cassante: la neotectonique et failles du massif de l'Ida (Crète), Grèce. Ann. Soc. Géol. Nord 95, 183–200.

Avnaim-Katav, S., Herut, B., Rahav, E., Katz, T., Weinstein, Y., Alkalay, R., Berman-Frank, I., Zlatkin, O., Almogi-Labin, A., 2020. Sediment trap and deep sea coretop sediments as tracers of recent changes in planktonic foraminifera assemblages in the southeastern ultra-oligotrophic Levantine Basin. Deep-Sea Res. II 171, 104669. https://doi.org/10.1016/j.dsr2.2019.104669.

Bemis, B.E., Spero, H.J., Bijma, J., Lea, D.W., 1998. Reevaluation of the oxygen isotopic composition of planktonic foraminifera: experimental results and revised paleotemperature equations. Paleoceanography 13 (2), 150–160. https://doi.org/10.1029/98PA00070.

Bizon, J.-J., Bizon, G., 1965. L'Helvétien et le Tortonien de la région de Parga (Epire continentale, Grèce). Rev. Micropaleontol. 7, 242–256.

Blow, W.H., 1959. Age, correlation and biostratigraphy of the upper Tocuyo (San Lorenzo) and Pozon formation, eastern Falcon, Venezuela. Bull. Am. Pal. 39 (178), 67–251.

Bosmans, J.H.C., Hilgen, F.J., Tuenter, E., Lourens, L.J., 2015a. Obliquity forcing of low-latitude climate. Clim. Past 11, 1335–1346. https://doi.org/10.5194/cp-11-1335-2015.

Bosmans, J.H.C., Drijfhout, S.S., Tuenter, E., Hilgen, F.J., Lourens, L.J., Rohling, E.J., 2015b. Precession and obliquity forcing of the freshwater budget over the Mediterranean. Quat. Sci. Rev. 123, 16–30. https://doi.org/10.1016/j.quascirev.2015.06.008.

Bosmans, J., van der Ent, R.J., Haarmsa, R., Drijfhout, S.S., Hilgen, F.J., 2020. Precession- and obliquity-induced changes in moisture sources for enhanced precipitation over the Mediterranean Sea. Paleoceanogr. Paleocl. 35 https://doi.org/10.1029/2019PA003655 e2019PA003655.

Brady, H.B., 1882. Report on the Foraminifera. In: Tizard, Murray, J. (Eds.), Exploration of the Faroe Channel during the summer of 1880, in her Majesty's hired Ship "knight Errant". R. Soc. Edinburgh, 111, pp. 708–717. Edinburgh.

Catalano, R., Sprovieri, R., 1971. Biostratigrafia di alcune serie Saheliane (Messiniano inferiore) in Sicilia. In: Farinacci, A., Matteucci, R. (Eds.), Proceedings of the Second Planktonic Conference, Roma 1970. Edizioni Tecno-Scienza, Rome, pp. 211–249.

Conato, V., 1964. Alcuni Foraminiferi nuovi nel Pliocene nord-appenninico. Contributo 1. Geol. Rom. 3, 279–302.

Cox, K.A., Rohling, E.J., Schmidt, G.A., Schiebel, R., Bacon, S., Winter, D.A., Bolshaw, M., Spero, H.J., 2011. New constraints on the Eastern Mediterranean $\delta^{18}O$: δD relationship. Ocean Sci. Discuss. 8, 39–53. https://doi.org/10.5194/osd-8-39-2011.

Creutzburg, N., Papastamatiou, J., Sannemann, W., Seidel, E., Tataris, A., 1977. General Geological Map of Greece; Crete Island, 1:200,000. Institute of Geological and Mining Research (IGME), Athens.

De Boer, B., Peters, M., Lourens, L.J., 2021. The transient impact of the African monsoon on Plio-Pleistocene Mediterranean sediments. Clim. Past 17, 331–344. https://doi.org/10.5194/cp-17-331-2021.

Delrieu, B., 1990. Evolution tectono-sédimentaire du Malevisi et du secteur d'Ano Moulia au Miocène Supérieur (Bassin d'Héraklion, Crète Centrale, Grèce). Mem. Géol. IGAL 42, 1–369.

Drury, A.J., Westerhold, T., Hodell, D., Röhl, U., 2018. Reinforcing the North Atlantic backbone: revision and extension of the composite splice at ODP Site 982. Clim. Past 14, 321–338. https://doi.org/10.5194/cp-14-321-2018.

Fairbanks, R.G., Wiebe, P.H., 1980. Foraminifera and chlorophyll maximum: vertical distribution, seasonal succession, and paleoceanographic significance. Science 209, 1524–1526. https://doi.org/10.1126/science.209.4464.1524.

Fairbanks, R.G., Sverdlove, M., Free, R., Wiebe, P.H., Bé, A.W.H., 1982. Vertical distribution of living planktonic foraminifera from the Panama Basin. Nature 298, 841–844. https://doi.org/10.1038/298841a0.

Fassoulas, C., 2001. The tectonic development of a Neogene basin at the leading edge of the active European margin: the Heraklion Basin, Crete. Greece. J. Geodyn. 31, 49–70. https://doi.org/10.1016/S0264-3707(00)00017-X.

Filippelli, G.M., Sierro, F.J., Flores, J.A., Vazques, A., Utrilla, R., Perez-Folgado, M., Latimer, J.C., 2003. A sediment-nutrient-oxygen feedback responsible for productivity variations in Late Miocene sapropel sequences of the western Mediterranean. Palaeogeogr. Palaeoclimatol. Palaeoecol. 190, 335–348.

Gaudant, J., Fourtanier, E., Lauriat-Rage, A., Tsagaris, S., Vénec-Peyré, M., Zorn, I., 1997. Découverte d'une ichthyofauna marine dans le Messinien préévaporitique de la Messara (Crète centrale, Grèce): interprétation paléoécologique. Géologie Méditerranéene 24 (3-4, 175–195.

Govers, R., Wortel, M.J.R., 2005. Lithosphere tearing at STEP faults: response to edges of subduction zones. Earth Planet. Sci. Lett. 236, 505–523. https://doi.org/10.1016/j.epsl.2005.03.022.

Hilgen, F., Krijgsman, W., 1999. Cyclostratigraphy and astrochronology of the Tripoli diatomite Formation (pre-evaporite Messinian, Sicily, Italy). Terra Nova 11, 16–22. https://doi.org/10.1046/j.1365-3121.1999.00221.x.

Hilgen, F.J., Krijgsman, W., Langereis, C.G., Lourens, L.J., Santarelli, A., Zachariasse, W. J., 1995. Extending the astronomical (polarity) time scale into the Miocene. Earth Planet. Sci. Lett. 136, 495–510. https://doi.org/10.1016/0012-821X(95)00207-S.

Hilgen, F., Krijgsman, W., Wijbrans, J.R., 1997. Direct comparison of astronomical and $^{40}Ar/^{39}Ar$ ages of ash beds: potential implications for the age of mineral dating standards. Geophys. Res. Lett. 24 (16), 2043–2046. https://doi.org/10.1029/97GL02029.

Hilgen, F.J., Bissoli, L., Iaccarino, S., Krijgsman, W., Meijer, R., Negri, A., Villa, G., 2000. Integrated stratigraphy and astrochronology of the Messinian GSSP at Oued Akrech (Atlantic Morocco). Earth Planet. Sci. Lett. 182 (3–4), 237–251. https://doi.org/10.1016/S0012-821X(00)00247-8.

Hodell, D., Curtis, J., Sierro, F.J., Raymo, M., 2001. Correlation of Late Miocene-to-early Pliocene sequences between the Mediterranean and North Atlantic. Paleoceanography 16, 164–178. https://doi.org/10.1029/1999PA000487.

IGME, 1994. Geological Map of Greece, Sheet Epano Archanae. Institute of Geology and Mineral Exploration (IGME), Athens.

IGME, 1996. Geological Map of Greece at Scale 1:50.000, Sheet Heraklion. Institute of Geology and Mineral Exploration (IGME), Athens.

Jenkins, D.G., 1960. Planktonic foraminifera from the Lakes Entrance oil shaft, Victoria, Australia. Micropaleontology 6, 345–371.

Jonkers, H.A., 1984. Pliocene benthonic foraminifera from homogeneous and laminated marls on Crete. Utrecht Micropal. Bull. 31, 1–179.

Jonkers, L., Kučera, M., 2015. Global analysis of seasonality in the shell flux of extant planktonic Foraminifera. Biogeosciences 12, 2207–2226. https://doi.org/10.5194/bg-12-2207-2015.

Juggins, S., 2003. Software for Ecological and Palaeoecological Data Analysis and Visualization. Tutorial version 1.3 [C2 Home (ncl.ac.uk)].

Kassis, D., Korres, G., 2020. Hydrography of the Eastern Mediterranean basin derived from Argo floats profile data. Deep-Sea Res. II: Topical Studies. Oceanography 171, 104172. https://doi.org/10.1016/j.dsr2.2019.104712.

Kennett, J.P., 1966. The *Globorotalia crassaformis* bioseries in North Westland and Marlborough, New Zealand. Micropaleontology 12, 235–245.

Kouwenhoven, T., Seidenkrantz, M.S., Van der Zwaan, G.J., 1999. Deep-water changes: the near-synchronous disappearance of a group of benthic foraminifera from the Late Miocene Mediterranean. Palaeogeogr. Palaeoclimatol. Palaeoecol. 152, 259–281. https://doi.org/10.1016/S0031-0182(99)00065-6.

Krijgsman, W., Hilgen, F., Langereis, C.G., Santarelli, A., Zachariasse, W.J., 1995. Late Miocene magnetostratigraphy, biostratigraphy and cyclostratigraphy in the Mediterranean. Earth Planet. Sci. Lett. 136, 475–494. https://doi.org/10.1016/0012-821X(95)00206-R.

Krijgsman, W., Hilgen, F., Raffi, I., Sierro, F.J., Wilson, D.S., 1999. Chronology, causes and progression of the Messinian salinity crisis. Nature 400, 652–655. https://doi.org/10.1038/23231.

Krijgsman, W., Capella, W., Simon, D., Hilgen, F.J., Kouwenhoven, T.J., Meijer, P.Th., Sierro, F.J., Tulbure, M.A., van den Berg, B.C.J., van der Schee, M., Flecker, R., 2018. The Gibraltar Corridor: Watergate of the Messinian Salinity Crisis. Mar. Geol. 403, 238–246. https://doi.org/10.1016/j.margeo.2018.06.008.

Laskar, J., Robutel, P., Joutel, F., Gastineau, M., Correia, A.C.M., Levrard, B., 2004. A longterm numerical solution for the insolation quantities of the Earth. Astron. Astrophys. 428, 261–285. https://doi.org/10.1051/0004-6361:20041335.

Lourens, L.J., Hilgen, F.J., Gudjonsson, L., Zachariasse, W.J., 1992. Late Pliocene to early Pleistocene astronomically forced sea surface productivity and temperature variations in the Mediterranean. Mar. Micropal. 19, 49–78. https://doi.org/10.1016/0377-8398(92)90021-B.

Lourens, L.J., Antonarakou, A., Hilgen, F.J., Van Hoof, A.A.M., Vergnaud Grazzini, C., Zachariasse, W.J., 1996. Evaluation of the Plio-Pleistocene astronomical timescale. Paleoceanography 11, 391–413. https://doi.org/10.1029/96PA01125.

Lourens, L.J., Hilgen, F.J., Raffi, I., 1998. 15. Base of large *Gephyrocapsa* and astronomical calibration of early Pleistocene sapropels in Site 967 and Hole 969D: Solving the chronology of the Vrica section (Calabria, Italy). In: Robertson, A.H.F., Emeis, K.-C., Richter, C., Camerlenghi, A. (Eds.), Proceeding of the Ocean Drilling Program, Scientific Results, vol. 160, pp. 191–197. https://doi.org/10.2973/odp.proc.sr.160.017.1998.

Lourens, L., Wehausen, R., Brumsack, H., 2001. Geological constraints on tidal dissipation and dynamical ellipticity of the Earth over the past three million years. Nature 409 (6823), 1029–1033. https://doi.org/10.1038/35059062.

Moissette, P., Cornée, J.J., Antonarakou, A., Kontakiotis, G., Drinia, H., Koskeridou, E., Tsourou, T., Agiadi, K., Karakitsios, V., 2018. Palaeoenvironmental changes at the Tortonian/Messinian boundary: a deep-sea sedimentary record of the eastern Mediterranean Sea. Palaeogeogr. Palaeoclimatol. Palaeoecol. 505, 217–233. https://doi.org/10.1016/j.palaeo.2018.05.046.

Nijenhuis, I.A., Schenau, S.J., Van Der Weijden, C.H., Hilgen, F.J., Lourens, L.J., Zachariasse, W.J., 1996. On the origin of upper Miocene sapropelites: a case study from the Faneromeni Section, Crete (Greece). Paleoceanography 11, 633–645. https://doi.org/10.1029/96PA01963.

Ogniben, L., 1958. Stratigrafie e microfaune del Terziario della zona di Caiazzo (Caserta), 6; descrizione paleontologiche. Riv. Ital. Paleontol. Stratigr. 64, 89–286.

Paillard, D., Labeyrie, L., Yiou, P., 1996. Macintosh program performs time-series analysis. Eos Trans. AGU 77 (39), 379. https://doi.org/10.1029/96EO00259.

Pellegrino, L., Dela Pierre, F., Natalicchio, M., Carnevale, G., 2018. The Messinian diatomite deposition in the Mediterranean region and its relationship to the global silica cycle. Earth-Sci. Rev. 178, 154–176.

Pellegrino, L., Abe, K., Gennari, R., Lozar, F., Dela Pierre, F., Natalicchio, M., Mikami, Y., Jordan, R.W., Carnevale, G., 2020. Integrated micropaleontological study of the Messinian diatomaceous deposits of the Monferrato Arc (Piedmont basin, NW Italy): New insights into the paleoceanographic evolution of the northernmost Mediterranean region. Mar. Geol. 160, 101910.

Perconig, E., 1968. Nuove specie di foraminiferi planctonici della Sezione di Carmona (Andalusia, Spagna). CMNS, Giorn. Geologia 35 (3), 219–232.

Pérez-Folgado, M., Sierro, F.J., Bàrcena, M.A., Flores, J.A., Vàzquez, A., Utrilla, R., Hilgen, F.J., Krijgsman, W., Filippelli, G.M., 2003. Western versus eastern Mediterranean paleoceanographic response to astronomical forcing: a high-resolution microplankton study of precession-controlled sedimentary cycles during the Messinian. Palaeogeogr. Palaeoclimatol. Palaeoecol. 190, 317–334. https://doi.org/10.1016/S0031-0182(02)00612-0.

Pierre, C., 1999. The oxygen and carbon isotope distribution in the Mediterranean water masses. Mar. Geol. 153, 41–55. https://doi.org/10.1016/S0025-3227(98)00090-5.

Prell, W.L., Curry, W.B., 1981. Faunal and isotopic indices of monsoonal upwelling - western Arabian Sea. Oceanol. Acta 4 (1), 91–98. https://archimer.ifremer.fr/doc/00121/23240/.

Pujol, C., Vergnaud Grazzini, C., 1995. Distribution patterns of live planktic foraminifers as related to regional hydrography and productive systems of the Mediterranean Sea. Mar. Micropaleontol. 25, 187–217. https://doi.org/10.1016/0377-8398(95)00002-I.

Roberts, G.G., White, N.J., Shaw, B., 2013. An uplift history of Crete, Greece, from inverse modeling of longitudinal river profiles. Geomorphology 198, 177–188. https://doi.org/10.1016/j.geomorph.2013.05.026.

Rohling, E.J., Gieskes, W.W.C., 1989. Late Quaternary changes in Mediterranean Intermediate Water density and formation rate. Paleoceanography 4, 531–545. https://doi.org/10.1029/PA004i005p00531.

Rohling, E.J., Jorissen, F.J., Vergnaud Grazzini, C., Zachariasse, W.J., 1993. Northern Levantine and Adriatic Quaternary planktic foraminifera; Reconstruction of paleoenvironmental gradients. Mar. Micropal. 21 (1–3), 191–218. https://doi.org/10.1016/0377-8398(93)90015-P.

Rohling, E.J., Marino, G., Grant, K.M., 2015. Mediterranean climate and oceanography, and the periodic development of anoxic events (sapropels). Earth-Sci. Rev. 143, 62–97. https://doi.org/10.1016/j.earscirev.2015.01.008.

Schenau, S.J., Antonarakou, A., Hilgen, F.J., Lourens, L.J., Nijenhuis, I.A., Van Der Wejden, C.H., Zachariasse, J.W., 1999. Organic rich layers in the Metochia section (Gavdos, Greece): evidence for a single sapropel formation mechanism in the eastern Mediterranean during the last 10 Myr. Paleoceanography 153, 117–135.

Seidenkrantz, M.S., Kouwenhoven, T.J., Jorissen, F.J., Shackleton, N.J., Van der Zwaan, G.J., 2000. Benthic foraminifera as indicators of changing Mediterranean–Atlantic water exchange in the late Miocene. Mar. Geol. 163 (1), 387–407. https://doi.org/10.1016/S0025-3227(99)00116-4.

Shackleton, N.J., 1974. Attainment of isotopic equilibrium between ocean water and the benthonic foraminifera genus *Uvigerina*: isotopic changes in the ocean during the last glacial. Colloques Internationaux du C.N.R.S. 219, 203–209.

Sierro, F.J., Flores, J.A., Civis, J., Gonzales Delgado, J.A., Frances, G., 1993. Late Miocene globorotaliid event-stratigraphy and biogeography in the NE Atlantic and Mediterranean. Mar. Micropal. 21, 143–168.

Sierro, F.J., Flores, J.A., Frances, G., Vazquez, A., Utrilla, R., Zamarreno, I., Erlenkeuser, H., Barcena, M.A., 2003. Orbitally-controlled oscillations in planktic communities and cyclic changes in western Mediterranean hydrography during the Messinian. Palaeogeogr. Palaeocl. Palaeoecol. 190, 289–316. https://doi.org/10.1016/S0031-0182(02)00611-9.

Sissingh, W., 2008. Punctuated Neogene tectonics and stratigraphy of the African-Iberian plate-boundary zone: concurrent development of Betic-Rif basins (southern Spain, northern Morocco). Neth. J. Geosci. - Geologie En Mijnbouw 87 (4), 241–289. https://doi.org/10.1017/S0016774600023350.

Spaak, P., 1983. Accuracy in correlation and ecological aspects of the planktonic foraminiferal zonation of the Mediterranean Pliocene. Utrecht Micropal. Bull. 28, 1–159.

Ten Veen, J.H., Postma, G., 1999a. Neogene tectonics and basin fill patterns in the Hellenic outer-arc (Crete, Greece). Basin Res. 11, 223–241. https://doi.org/10.1046/j.1365-2117.1999.00097.x.

Ten Veen, J.H., Postma, G., 1999b. Roll-back controlled vertical movements of outer arc basins of the Hellenic subduction zone (Crete, Greece). Basin Res. 11, 243–266. https://doi.org/10.1046/j.1365-2117.1999.00098.x.

Tjalsma, R.C., 1971. Stratigraphy and foraminifera of the Neogene of the eastern Guadalquivir Basin (Southern Spain). Utrecht Micropal. Bull. 4, 1–161.

Torrence, C., Compo, G.P., 1998. A practical guide to wavelet analysis. Bull. Amer. Meteor. Soc. 79, 61–78. http://paos.colorado.edu/research/wavelets.

Van der Zwaan, G.J., Jorissen, F.J., de Stigter, H.C., 1990. The depth dependency of planktonic/benthic foraminiferal ratios: Constraints and applications. Mar. Geol. 95, 1–16. https://doi.org/10.1016/0025-3227(90)90016-D.

Van Hinsbergen, D.J.J., Meulenkamp, J.E., 2006. Neogene supradetachment basin development on Crete (Greece) during exhumation of the South Aegean core complex. Basin Res. 18, 103–124. https://doi.org/10.1111/j.1365-2117.2005.00282.x.

Van Hinsbergen, D.J.J., Kouwenhoven, T.J., Van Der Zwaan, G.J., 2005. Paleobathymetry in the backstripping procedure: Correction for oxygenation effects on depth estimates. Palaeogeogr. Palaeoclimatol. Palaeoecol. 221 (3), 245–265. https://doi.org/10.1016/j.palaeo.2005.02.013.

Walters, R., 1965. The *Globorotalia zealandica* and *G. miozea* lineages. New Zealand J. Geol. Geophys. 8, 109–127.

Zachariasse, W.J., 1975. Planktonic foraminiferal biostratigraphy of the late Neogene of Crete (Greece). Utrecht Micropal. Bull. 11, 1–171.

Zachariasse, W.J., 1979. Planktonic foraminifera from section Potamidha I: Taxonomic and phyletic aspects of keeled globororotaliides and some paleoenvironmental estimates. Utrecht Micropal. Bull. 21, 129–165.

Zachariasse, W.J., Van Hinsbergen, D.J.J., Fortuin, A.R., 2008. Mass wasting and uplift on Crete and Karpathos during the early Pliocene related to initiation of South Aegean left-lateral, strike-slip tectonics. Geol. Soc. Am. Bull. 120, 976–993. https://doi.org/10.1130/B26175.1.

Zachariasse, W.J., Van Hinsbergen, D.J.J., Fortuin, A.R., 2011. Formation and fragmentation of a late Miocene supradetachment basin in Central Crete: implications for exhumation mechanisms of high-pressure rocks in the Aegean forearc. Basin Res. 23, 678–701. https://doi.org/10.1111/j.1365-2117.2011.00507.x.

Zhang, J., 1985. Living planktonic foraminifera from the eastern Arabian Sea. Deep-Sea Res. I 32 (7), 789–798. https://doi.org/10.1016/0198-0149(85)90115-3.